

Characterization of the human ESC transcriptome by hybrid sequencing

Kin Fai Au^a, Vittorio Sebastian^b, Pegah Tootoonchi Afshar^c, Jens Durruthy Durruthy^b, Lawrence Lee^{d,e}, Brian A. Williams^f, Harm van Bakel^g, Eric E. Schadt^g, Renee A. Reijo-Pera^b, Jason G. Underwood^{d,h,1}, and Wing Hung Wong^{a,1}

^aDepartment of Statistics and Department of Health Research and Policy, Stanford University, Stanford, CA 94305; ^bCenter for Human Pluripotent Stem Cell Research and Education, Department of Obstetrics and Gynecology, Institute for Stem Cell Biology and Regenerative Medicine, Stanford University School of Medicine, Stanford, CA 94305; ^cDepartment of Electrical Engineering, School of Engineering, Stanford University, Stanford, CA 94305; ^dPacific Biosciences of California, Menlo Park, CA 94025; ^eInvitae Inc., San Francisco, CA 94107; ^fDivision of Biology and Beckman Institute, California Institute of Technology, Pasadena, CA 91125; ^gDepartment of Genetics and Genomic Sciences, Mount Sinai School of Medicine, New York, NY 10029-6574; and ^hUniversity of Washington, Department of Genome Sciences, Seattle, WA 98105

Contributed by Wing Hung Wong, November 5, 2013 (sent for review August 6, 2013)

Although transcriptional and posttranscriptional events are detected in RNA-Seq data from second-generation sequencing, full-length mRNA isoforms are not captured. On the other hand, third-generation sequencing, which yields much longer reads, has current limitations of lower raw accuracy and throughput. Here, we combine second-generation sequencing and third-generation sequencing with a custom-designed method for isoform identification and quantification to generate a high-confidence isoform dataset for human embryonic stem cells (hESCs). We report 8,084 RefSeq-annotated isoforms detected as full-length and an additional 5,459 isoforms predicted through statistical inference. Over one-third of these are novel isoforms, including 273 RNAs from gene loci that have not previously been identified. Further characterization of the novel loci indicates that a subset is expressed in pluripotent cells but not in diverse fetal and adult tissues; moreover, their reduced expression perturbs the network of pluripotency-associated genes. Results suggest that gene identification, even in well-characterized human cell lines and tissues, is likely far from complete.

isoform discovery | PacBio | hESC transcriptome | alternative splicing | lncRNA

In the 5 y since the introduction of RNA-Seq (1, 2), there have been remarkable advances in our ability to analyze the transcriptome. During this period, additional methods based on next-generation sequencing (NGS) have been developed for the study of many different aspects of RNA biology. These include methods to study RNA species that are ribosome bound (3), nuclear (4), implicated in RNA editing (5), functional noncoding RNAs (6), in protein–RNA binding sites (7), and interacting in microRNA–mRNA complexes (8). Concurrently, the increase in NGS throughput and the development of multiplex sequencing protocols have made RNA-Seq analysis as cost-effective as gene expression microarrays.

Despite these advances, we are still far from achieving the original goals of RNA-Seq analysis, namely the de novo discovery of genes, the assembly of gene isoforms, and the accurate estimation of transcript abundance at the gene or the isoform level. Current RNA-Seq experiments are based on second-generation sequencing (SGS) instruments capable of generating a large number of short reads. From these reads, one obtains two types of information: (*i*) frequency of reads aligned to a contiguous genomic segment (exonic reads) and (*ii*) frequency of reads aligned to two contiguous segments of the genome with a single gap of from 60 bp to 400 kbp in size (junction reads) (9–11). If the set of possible isoforms is assumed known (i.e., the gene is well annotated), then it is possible to infer isoform-specific expression from exonic reads and junction reads based on simple statistical models such as the Poisson deconvolution model of Jiang and Wong (12). On the other hand, if the set of isoforms is not known or only partially known, then currently there is great

difficulty in isoform quantification based on SGS data. The main reason is due to insufficient length of the SGS reads. The median length of human gene transcripts is about 2,500 bp, which is much longer than the length of a contiguous read (about 250 bp) currently attainable by SGS. In previous work we showed that generally, isoform deconvolution from short-read RNA-Seq data is not an identifiable problem (13), in the sense that isoform expression cannot always be uniquely determined from the set of exons and splice junctions. Thus, strong assumptions are made on the set of candidate isoforms in all current methods for isoform assembly from short reads, including Cufflinks (14), SLIDE (15), and Montebello (16); as a result, the assembled isoforms are of uncertain accuracy. Although hundreds of RNA-Seq datasets are being generated in any given day by diverse groups in academia and industry, their interpretations all depend critically on the completeness and reliability of gene and isoform annotations on the species and cell types being analyzed. Although results from *de novo* transcript reconstruction algorithms can provide useful hints, they are not accurate enough to stand on their own as definitive evidence for new transcripts.

One may hope that the completeness and reliability of gene annotation are improving commensurably with the exponential increase in the amount and diversity of sequence data from RNA-Seq. However, from release 43 (September 2010) to 49

Significance

Isoform identification and discovery are an important goal for transcriptome analysis because the majority of human genes express multiple isoforms with context- and tissue-specific functions. Better annotation of isoforms will also benefit downstream analysis such as expression quantification. Current RNA-Seq methods based on short-read sequencing are not reliable for isoform discovery. In this study we developed a new method based on the combined analysis of short reads and long reads generated, respectively, by second- and third-generation sequencing and applied this method to obtain a comprehensive characterization of the transcriptome of the human embryonic stem cell. The results showed that large gain in sensitivity and specificity can be achieved with this strategy.

Author contributions: K.F.A. and W.H.W. designed research; K.F.A., V.S., P.T.A., J.D.D., H.V.B., R.A.R.-P., and J.G.U. performed research; K.F.A., L.L., B.A.W., and E.E.S. contributed new reagents/analytic tools; K.F.A. analyzed data; and K.F.A. and W.H.W. wrote the paper.

The authors declare no conflict of interest.

Freely available online through the PNAS open access option.

Data deposition: The data reported in this paper have been deposited in the Gene Expression Omnibus (GEO) database, www.ncbi.nlm.nih.gov/geo (accession no. [GSE51861](#)).

¹To whom correspondence may be addressed. E-mail: whwong@stanford.edu or jundy@uw.edu.

This article contains supporting information online at www.pnas.org/lookup/suppl/doi:10.1073/pnas.1320101110/-DCSupplemental.

(September 2011), the number of RefSeq records for mammals increased by 6.4% (17). Does this slow increase imply that the annotations of mammalian transcripts are close to complete? We believe the answer is clearly negative. The slow increase is likely due to underinvestment in new tools and methods to generate full-length transcript sequences. Even in well-studied species such as human and mouse, isoforms with low to moderate abundance are only partially sampled in full-length cDNA sequencing, especially when their expression is specific to a minority of cell types. Ironically, although gene annotations are necessary for the interpretation of short-read RNA-Seq data, the emergence of RNA-Seq itself as the preferred method to examine the transcriptome may be contributing to a slowdown of large-scale cDNA and EST sequencing projects that were once major sources of experimental evidence for gene annotation. This is a fundamental roadblock for further progress in transcriptomic analysis.

The research reported here offers a way out of this impasse. We address the hypothesis that full-length and large partial fragments of transcripts can be sequenced in a massively parallel fashion by combining SGS and third-generation sequencing (TGS). One characteristic of TGS technologies is that they can generate long reads. Pacific Biosciences (PacBio) RS, the first TGS platform to offer very long reads, has an average read length of 2–3 kb and reads of >7 kb are not uncommon (18). Thus, the use of TGS for transcript assembly has always been viewed as an attractive approach. In our preliminary work on this problem, we found that the major barriers in using PacBio for transcriptomic analysis are the relatively high error rate (up to 15%) and moderate throughput [50,000 reads per single molecule real time (SMRT) cell]. To bypass the first barrier, we developed a method to correct errors in PacBio long reads by SGS short reads from the same transcriptome (19). Here, we address the second barrier by proposing new statistical methods for transcript discovery and reconstruction based on the combined information from error-corrected long reads and short-read counts.

We applied our “hybrid sequencing” RNA-Seq method to human embryonic stem cells (hESCs), using the well-characterized H1 hESC line; this line is a Tier 1 ENCODE line whose transcriptome has been extensively studied by EST sequencing (20) and RNA-Seq (21–23). However, even for such a well-characterized cell line, our analysis revealed that its current annotation is very incomplete and there are hundreds of novel genes/long noncoding RNAs (lncRNAs) and thousands of novel isoforms of known genes expressed. In this paper we use the term “novel gene/isoform” to describe a gene loci or gene isoform that is directly detected by PacBio long reads or predicted by our proposed method in the H1 transcriptome, and not found in existing gene annotation databases [RefSeq, Ensembl (24), UCSC Known Genes (25), EST (26) and GENCODE(27)]. The lncRNAs identified by our study are on average much longer and have more exons than those annotated in existing databases, suggesting significant downward bias in the current strategy for genome-wide discovery of lncRNAs. Finally, our experimental validation demonstrated that at least a subset of novel transcripts represents bona fide gene loci.

Results

Gene Isoform Detection and Prediction. We applied the splice junction detection program SpliceMap (9) to 116,476,819 mappable 100-bp Illumina sequence reads and detected 183,825 junctions with an estimated false positive rate (FPR) of 5% (9). Of the detected junctions, 46,898 (~25.51%) were not reported in RefSeq. Furthermore, many of them were found in the intergenic regions and formed 2,568 clusters (*SI Appendix: Methods, Short Reads Alignment and Exon Junction Detections by SpliceMap*). This suggested that existing gene annotations are incomplete and there may exist many novel genes as well as novel isoforms of annotated genes.

To capture multiexon transcripts, we used the PacBio RS sequencing platform to capture the full-length RNA in hESCs (H1 cell line). We generated full-length cDNA libraries by two dif-

ferent established methods, using polyA RNA as starting material. The prepared double-stranded cDNA was then converted to libraries for PacBio single-molecule real-time sequencing. In total, 7,816,704 raw PacBio RS reads were generated. Error correction of the raw PacBio RS reads was performed by LSC (19). A total of 1,998,716 error-corrected long reads (GSE51861) were mappable to the reference human genome hg19 by BLAT. A total of 781,128 long reads covered at least one junction supported by SpliceMap junction detection or RefSeq annotation. In total, 8,084 gene transcript isoforms from RefSeq were detected directly with a full-length read. We compared these isoforms to the 5,851 multiexon RefSeq genes that are significantly expressed [i.e., having reads per kilobase per million mapped reads (RPKM) >10 based on Illumina short reads] in hESCs and found that although 61.37% of these genes are covered by the directly detected isoforms, the detection rate varies depending on the gene length. The detection rate is 78.18% (3,226) in the 3,689 multiexon genes of size <3,000 bp and 32.71% (707) in the 2,162 multiexon genes of size >3,000 bp (Fig. 1D). Although we also detected many single-exon transcripts, isoform identification of multiexon genes was of more interest for this study and we focused on those cases. Unless otherwise specified, the term “isoform” in the remaining text refers to multiexon RNA isoforms.

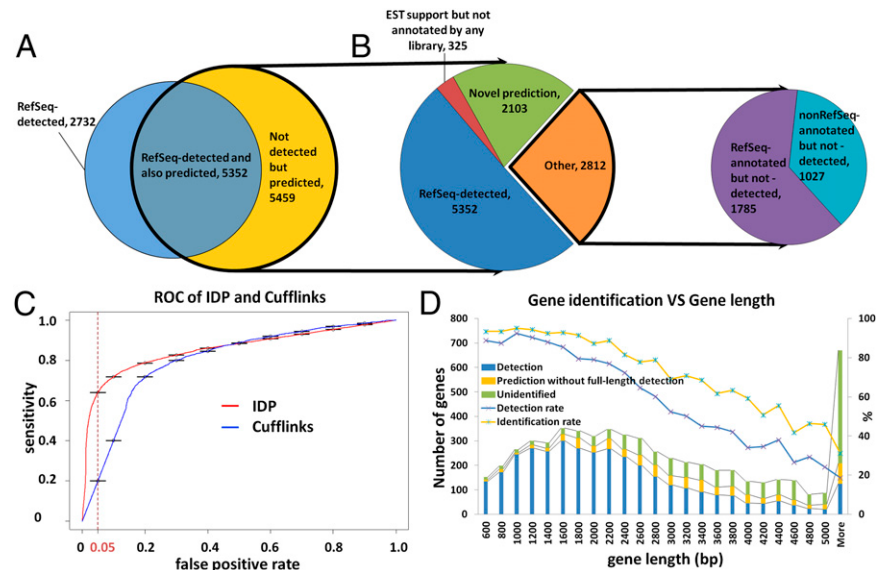
To identify more isoforms for long genes, we developed a statistical isoform prediction method to construct possible isoform candidates from the union of long reads and short reads with spliced alignment (*SI Appendix: Methods, IDP—Isoform Detection and Prediction*) (<http://www.stanford.edu/people/kinfai/IDP/IDP.html>). Using this method we obtained 5,459 isoform predictions (Fig. 1A), which significantly expanded the sensitivity of isoform identification beyond direct detection. We indicated a RefSeq isoform as identified by IDP if either it was directly detected by sequencing or there was a predicted isoform with an identical set of exon–exon junctions. The isoform-based identification rate of significantly expressed genes now improved to 73.70% (compared with 61.4% by direct detection). More specifically, for long genes (>3,000 bp) the identification rate improved from 32.70% to 50.23%, whereas for short genes (<3,000 bp) the identification rate improved from 71% to 90% (Fig. 1D). As we keep optimizing LSC and IDP, we will keep updating the hESC transcriptome at our website (<http://www.stanford.edu/people/kinfai/IDP/hESC.html>), including novel isoforms, novel genes, novel lncRNA, and gene/isoform profiling.

We compared the performance of IDP isoform prediction against Cufflinks, which is currently the most widely used method for isoform identification based on short reads [Fig. 1C; see *SI Appendix* for details of receiver operating characteristic (ROC) analysis]. At the same specificity of 5% false positive rate, IDP had a much higher sensitivity (62% true positive) compared with Cufflinks (20% true positive). This result shows that IDP is effective in using the information from the PacBio long reads to significantly improve isoform identification.

The predicted (i.e., not directly detected) isoforms from IDP included a large number of annotated isoforms that are from RefSeq (1,785 isoforms) or other annotation libraries [1,027 isoforms; combined Ensembl, GENCODE, and University of California, Santa Cruz (UCSC) Known Genes]. There is also a small group (325) of nonannotated but EST-supported isoforms. More importantly, 2,103 predicted isoforms are not reported by any existing annotations. The identification of these isoforms provides a more comprehensive characterization of the hESC transcriptome. As discussed below, the novel isoforms also lead to better estimates of isoform-specific gene expression.

Novel Genes. Of the 2,103 identified novel isoforms that are not reported by any existing annotations, 273 isoforms were transcribed from 216 novel nonannotated gene loci, i.e., all of the splicing junctions are not reported in any existing annotations (Fig. 2A). Using the short-read data, we computed their representation in RNA-Seq data from 16 adult human tissues (50 bp;

Fig. 1. Gene isoform detection and prediction of hESCs (H1 cell line) by IDP. (A) Venn diagram of IDP detections and predictions (see introductory section for definition of detection and prediction). A total of 8,084 RefSeq isoforms are detected and highlighted in blue. A total of 10,811 predictions are highlighted in yellow and outlined with a thick black line. A total of 5,352 detections of RefSeq isoforms are also predicted by IDP. (B) Pie chart of annotated isoforms and novel isoforms in IDP predictions. IDP predictions rescue 1,785 RefSeq-annotated isoforms (in purple) that cannot be detected directly at full length. In addition, there are 1,027 predictions that are not annotated in RefSeq but are found in Ensembl, Known Genes, or GENCODE (cyan). Finally, 2,428 novel isoforms (green and red) are identified, 325 of which have EST support (red). (C) ROC performance analysis of IDP and Cufflinks. IDP predictions have much higher sensitivity in the acceptable FPR range from 5% to 10%. When FPR is controlled to 5%, the IDP prediction sensitivity is as high as ~62%, whereas the corresponding Cufflinks sensitivity is only about 20%. (D) RefSeq gene identification rate decreases with the gene length. Combining detections and predictions, the overall identification rate by IDP is ~73% (yellow line with blue star markers). IDP prediction rescues a significant number of isoforms from long genes that are not directly detected.



Illumina Human Body Map) and their abundance ratio with respect to H1. We began by plotting the abundance ratios of the 10 novel genes with the highest expression; 8 of these 10 genes had <5% relative expression levels in all 16 adult tissues compared with hESCs, which indicated that their expression was highly specific to hESCs and thus they may be valuable candidates for novel pluripotency markers (Fig. 2C). For example, several long reads with up to four junctions were mapped to the locus chr6:167,641,267–167,660,912 (hg19, the same below), where no annotated genes in RefSeq, Ensembl, UCSC Known Genes, or GENCODE are reported. The long reads indicated complex expression from this locus with at least three different isoforms transcribed (Fig. 2D). The RPKM of this gene was 31.94 in hESCs, a value much higher than the averaged RPKM (0.53) in the other 16 adult tissues. For the other 2 novel genes (of 10), the expression level in 16 tissues was comparable to that of hESCs, and both of them had isoforms containing three or more junctions. Next, to determine the hESC-specific expression of all 216 novel genes, we calculated their abundance ratio (over the expression in the 16 adult tissues) and we plotted it vs. the SD of abundance ratios for each one. Sixty-eight percent of the novel genes (146/216) had an average abundance ratio smaller than 0.5 with SD smaller than 0.5 (inside the pink box in Fig. 2B), which indicated that they had relative specific expression in hESCs. Because their expression is specific to H1 hESCs, they may not have been easily identified in the previous research. We noted that 32% of the novel genes (70/216) were not hESC specific; they had comparable abundance in the other human tissues.

hESC-Specific Novel Genes. To confirm that the novel genes have expression specific to hESCs, we further characterized 23 of those showing the highest expression. For this purpose, we examined expression by quantitative PCR in two independent hESC lines (H1 and H9), one induced pluripotent stem cell (iPSC) line (iPSC line RiPSC.HUF1), and a collection of cDNAs obtained from different adult human tissues. All 23 targets, denoted as *HPAT* (*Human Pluripotent Associated Transcript*) genes, were abundantly expressed in the pluripotent cell lines (H1, H9, and RiPSC.HUF1) as opposed to adult tissues where they were either undetectable or expressed at very low levels (Fig. 3A and *SI Appendix*, Fig. S9A). Controls included genes whose expression is highly enriched in pluripotent stem cells and tissue-specific markers (*SI Appendix*, Fig. S9 B and C).

We also examined expression during human development, in single blastomeres of eight-cell embryos and in human blastocysts (Fig. 3B). We observed three different categories of expression: genes (*HPAT1*, *HPAT15*, and *HPAT19*) detected in the blastocysts but not in the eight-cell-stage blastomeres, genes abundantly expressed in both blastocysts and eight-cell embryos (*HPAT2* and *HPAT3*), and genes that were not expressed in either stage of preimplantation development; controls were as shown (*SI Appendix*, Fig. S9D). To further investigate the role of the genes in pluripotency, we also examined their expression during reprogramming of neonatal fibroblasts toward iPSCs. We observed that several of these genes, which were not expressed in parental fibroblasts, were activated during reprogramming (between day 10 and day 12) with a kinetic very similar to that observed for the pluripotency-associated genes like *NANOG*, *POU5F1*, and *DNMT3B* (Fig. 3C).

To confirm that the identified *HPAT* genes encoded functional elements, we performed knockdown experiments. For this purpose, we transfected H1 cells with siRNAs and analyzed gene expression 24 h posttransfection. Results indicated that reduction of the novel hESC-specific gene (*HPAT1*) resulted in significant down-regulation of expression of several pluripotency-associated factors including *POU5F1*, *SOX2*, *NANOG*, *DPPA3*, *DNMT3B*, *SALL4*, and *TDGF1*, in a fashion similar to that observed in a control sample where we down-regulated *POU5F1* by transfecting a pool of four commercially available siRNAs (Fig. 4). Other genes like *LIN28A*, *TERT*, and *UTF1* were not affected (Fig. 4), indicating a targeted effect of *HPAT1* on the transcriptional network of pluripotency genes. Interestingly, the down-regulation of *HPAT1* also resulted in down-regulation of approximately half of the novel genes whereas the other half were unaffected (*SI Appendix*, Fig. S10 A and B).

Novel Gene Isoforms. In addition to the novel genes, 655 identified isoforms contained both annotated junctions and novel junctions and thus represent novel isoforms of known genes. The novel junctions increase the diversity of the existing known isoforms. A total of 758 novel junctions from this subgroup of isoforms were categorized by type (Fig. 5A). Twenty-four percent and 25% of the novel junctions resulted from novel splice sites at the 5' end and the 3' end, respectively. Seven percent of the junctions accounted for intron retention events. Fifteen percent resulted from exon-skipping events. Nine novel junctions were defined “intergenic proximal” because they fell upstream or downstream

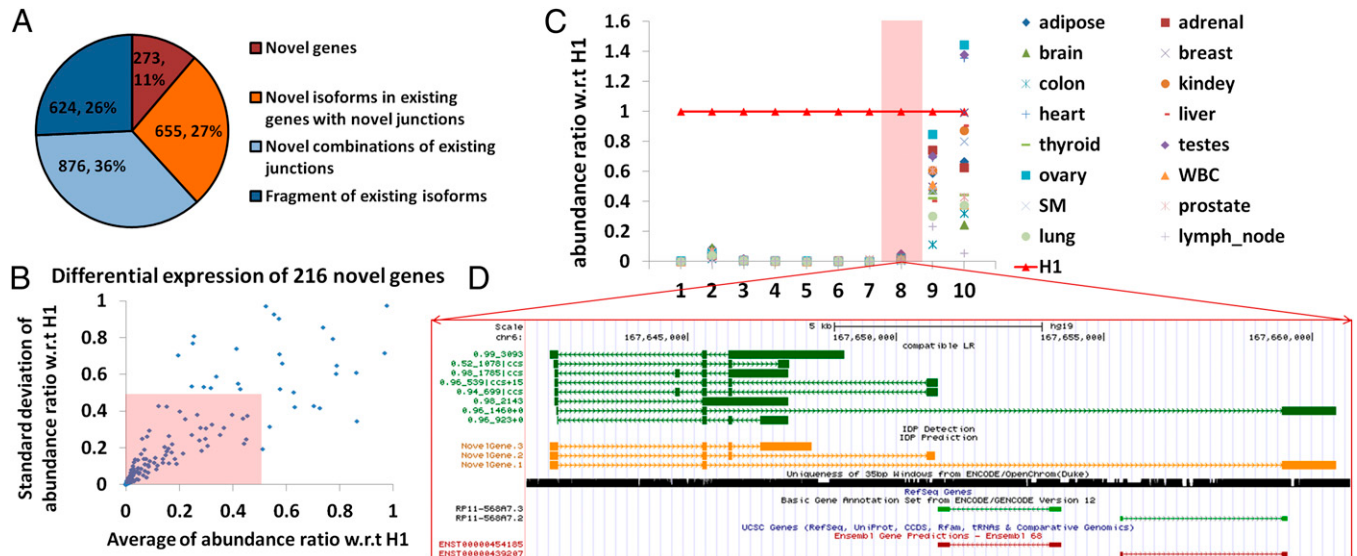


Fig. 2. Novel gene identifications. (A) A total of 2,428 novel isoforms are categorized according to the use of the annotated junctions. A total of 273 isoforms from 216 novel genes are observed (in brown). A total of 655 novel isoforms use at least one junction from annotated genes (in orange). A total of 876 novel isoforms are novel combinations of annotated junctions. Six hundred twenty-four are fragments of annotated isoforms. (B) Differential expression of 216 novel genes in H1. The abundance ratio of a novel gene in a given tissue is defined as its abundance in this tissue divided by its abundance in H1. One hundred forty-six novel genes (68%, inside the pink box) have an averaged abundance (among 16 human tissues) ratio smaller than 0.5 with SD smaller than 0.5. (C) Relative expression levels of the top 10 novel genes (10 highest expressions in hESCs) in 16 human tissues. The reference expression levels are expressions in hESCs (highlighted in red line with triangles). Eight novel genes have high expression specifically in hESCs (example 8 in D) whereas the other 2 have significant expression across many different tissues. The gene structure of the eighth novel gene is visualized in D. (D) Novel gene at chr6:167,641,267–167,660,912. The dark green track shows the nonredundant long reads, each of which represents an alignment. The arrow refers to the alignment of the read relative to the reference (i.e., aligned to reference or to reverse complement of reference) and is not the direction of transcription. The naming of nonredundant long reads is $A_B|ccs \pm D$, where A is the percentage identity of BLAT alignment, B is the length of alignment, and D is the distance between the mappable part of the long read and the polyA/polyT detection (“+” is the forward strand and downstream whereas “−” is the reverse strand and upstream). PacBio circular consensus sequence (CCS) reads are labeled with “ccs”. The orange track shows IDP predictions. The 35-bp mappability of this locus is in black. The light green track is GENCODE annotation and the brown one is Ensembl. RefSeq (light purple track) and UCSC Genes are also displayed but they have no annotated genes in this locus and thus no IDP detections (referenced to RefSeq, red track) are displayed either. The track display settings of other figures are the same.

of the annotated genes, thus extending the gene locus with novel exons and novel isoforms (Fig. 6). None of these novel splices have been reported in previous annotations.

Without any novel junctions, novel combinations of annotated junctions can generate novel isoforms as well. A total of 876 novel isoforms are identified in this category. This finding indicates that the completeness of junction libraries does not guarantee the completeness of gene isoform identification. Although SGS data have shown impressive performance in junction detection at local regions, new techniques such as IDP from hybrid-sequencing data are needed in isoform identifications.

Compared with annotated isoforms, the expression levels of the novel genes and novel isoforms identified by IDP are lower overall (Fig. 5B). However, a significant proportion (35.58%) have reasonably high expression levels ($RPKM > 10$). Thus, previous approaches have yielded incomplete annotations even for highly expressed genes. IDP will be useful in filling this gap.

Quantification of Isoform Abundance. Estimates of isoform-specific gene expression from high-throughput SGS data rely on statistical models in which a short read that is consistent with two or more of the annotated isoforms is regarded as being more likely to be generated from the more abundant isoforms (12). Isoform abundance estimates based on these models are highly sensitive to the annotation. Two types of isoform annotation libraries are often used: (i) reference annotation libraries such as RefSeq or Ensembl or (ii) candidate isoform sets inferred computationally by SGS analysis tools such as Cufflinks and SLIDE. Because a reference annotation library is constructed based on all data from the same species, not all annotated isoforms in the library are truly expressed in a sample. The inclusion of annotated but

not truly expressed isoforms can greatly increase the variability of the abundance estimates of the expressed isoforms—as discussed in section 4.2 of ref. 12, this shows up as a widening of the 95% interval for an isoform’s abundance when additional isoforms are included in the model. On the other hand, if the reference library is incomplete, then any nonannotated but truly expressed isoforms are completely missed and their contribution to short-read coverage may be incorrectly assigned to the annotated isoforms. These two effects can lead to serious errors in the abundance estimates based on a reference library. Finally, for multixon genes there are usually many isoforms consistent with the exon and junction reads from SGS data. As a result, candidate isoform sets inferred directly from the SGS data may include many false isoforms that cause incorrect abundance estimation. In contrast, in our approach the error-corrected long reads are ideal for narrowing down the isoforms expressed in a sample, thus enabling much more reliable abundance quantification from SGS reads.

To evaluate the bias in quantification due to incomplete annotation, we computed the isoform expression levels from SGS short reads based on two different isoform libraries: RefSeq annotation and IDP isoform identification from hESC data (Fig. 7). There are 9,775 isoforms appearing in both libraries (common isoforms). Of these, 1,763 are from genes with at least one novel isoform (group 1, with novel isoforms) and 8,012 are from genes without any novel isoform discoveries (group 2, without novel isoforms). For genes in group 2, the expression of a common isoform, computed via the RefSeq library, is well correlated with that computed based on the IDP library ($R^2 = 0.9985$). In contrast, for group 1 genes this correlation is much lower ($R^2 =$

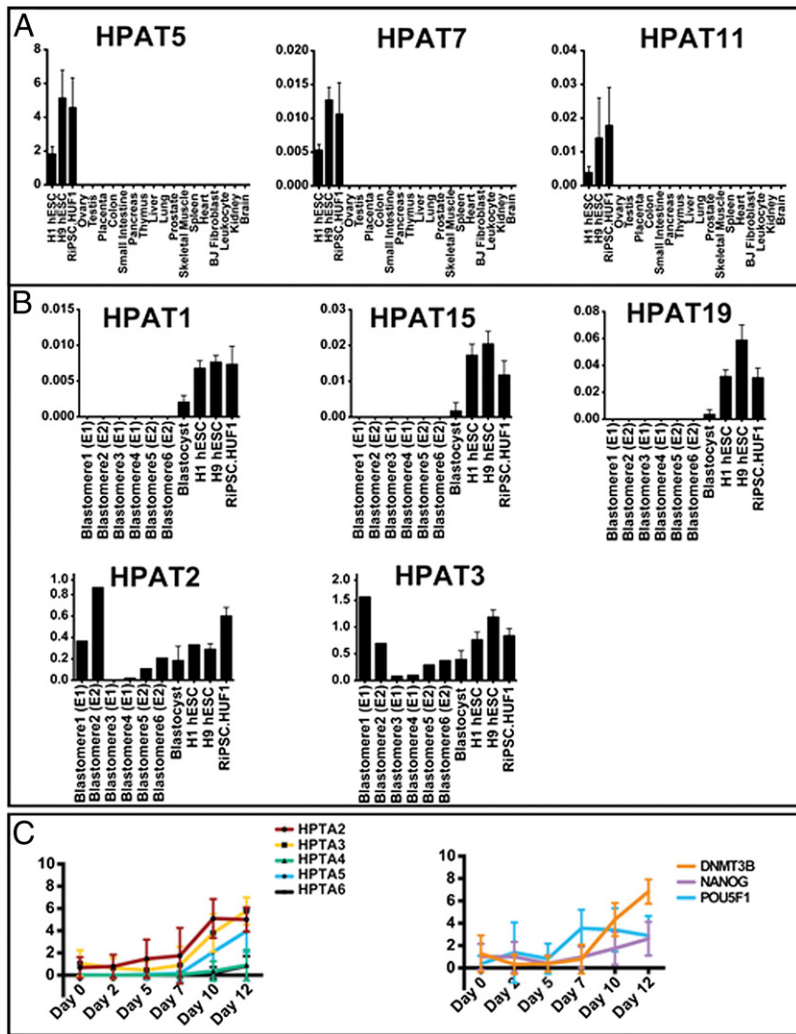


Fig. 3. Gene expression validation of HPAT. (A) Gene expression analysis by qPCR was performed on two hESC samples (H1 and H9), one iPSC line (RIPSC.HUF1), and a collection of cDNAs from fetal and adult tissues. (B) Gene expression profiling of HPAT genes in single blastomeres of eight-cell embryos and blastocysts. E1 and E2 denote the embryos from which blastomeres were isolated. (C) Reactivation of genes during the reprogramming process. Cells were analyzed at different time points of mRNA-mediated iPSCs derivation.

0.6008). Therefore, novel gene isoform discoveries have important effects in the accuracy of abundance estimations.

The linear regression of all 9,775 common isoforms shows the difference of abundance correction between group 1 and group 2 (Fig. 7). IDP-sample-specific estimations in group 1 genes tend to have lower RPKM because some SGS short reads must now be shared with the novel isoforms. This confirms that novel isoform identifications have a significant impact on the isoform abundance estimation within a gene. Therefore, our sample-specific IDP pipeline also leads to a more reliable isoform-specific expression estimation that will benefit downstream analyses.

Use of Gene Isoforms and Exon Junctions. Although there are ~20,000 multiexon genes with 35,000 ~ 40,000 isoforms in RefSeq, the total number of isoforms identified in hESCs is only 13,292. A total of 12,976 isoforms (RefSeq annotated or unannotated) were identified from 4,312 genes of 5,851 RefSeq multiexon genes with RPKM >10. The identification rate is 73.70% among these RefSeq genes (*Gene Isoform Detection and Prediction*). A total of 91.18% express only one or two dominantly expressed isoforms in hESCs (Fig. 8). Gene functions within a cell may depend only on a subset of possible isoforms. Thus, there must exist sophisticated transcriptional and posttranscriptional regulatory mechanisms to select and express a correct subset of isoforms in certain cell conditions. On the other hand, some genes express many isoforms in hESCs, such as 14 isoforms from the ncRNA gene NCRNA00188 and 13 from mortality factor MORF4L2.

In contrast to limited use of isoforms, the number of junctions used within a gene has a much larger range from 1 to 50. Thus, the IDP pipeline with hybrid sequencing data has identification power not only in simple genes but also in the complex genes with many alternative splices, such as the 49-junction gene RBM5 (RNA-binding protein 5) and the 50-junction gene DPP4 (adenosine deaminase complexing protein). This advantage of obtaining global gene structure with so many junctions is due to the TGS long reads and is not achievable by SGS short reads. In addition, the median number of junctions within a gene identified by IDP is 7, which is the same as in RefSeq annotation.

It is interesting to note, however, that the number of junctions within a gene has no significant correlation with the number of expressed isoforms (Fig. 8). This suggests that the number of expressed isoforms is largely determined by the need of the cell and does not depend on the complexity of the gene junctions.

Isoforms of Pluripotent Stem Cell Markers. Many genes are expressed with great specificity in hESCs. Reliable and sensitive gene isoform identification enables improved observation of the use of isoforms in hESCs. Here we report isoforms from 15 pluripotent stem cell markers (Table 1). As with most genes, these markers have significant expression of only one to two annotated isoforms, most of which can be detected directly by error-corrected full-length cDNA reads. Two annotated isoforms KLF4 and E-cadherin are the exceptions and are predicted by IDP.

The transcriptional regulator of pluripotency, POU5F1, expresses two isoforms, which are distinct from the RefSeq-annotated

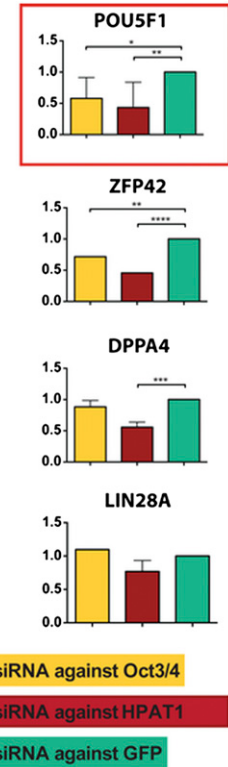


Fig. 4. Functional effect of down-regulation of HPAT genes. Gene expression analysis by qPCR of different pluripotency-associated genes after down-regulation of GFP (negative control, in green), OCT4 (positive control, in yellow), and HPAT1 (in red). siRNAs for GFP and HPAT1 were derived by in vitro dicer-mediated digestion of the corresponding double-stranded mRNAs; siRNAs for OCT4 were designed in silico. Analysis was performed 24 h after the transfection.

isoform NM_001173531. In addition, a few long reads are observed that exhibit intron retentions within two detected isoforms (NM_203289 and NM_002701). However, the corresponding intronic coverage is not high, so these intron retention events may be from preprocessed transcripts. Similar intron retention events with low expression also exist in NANOG, TERT, and DNMT3B.

Compared with intron retentions that occur at low frequency, novel isoforms with highly expressed exon-skipping events are more interesting. For example, in the DPPA4 locus, a RefSeq-annotated isoform is expressed but a novel isoform skipping three exons contributes ~17% of the total gene abundance (*SI Appendix, Fig. S11A*). In TERT, a novel isoform displaying cassette exon skipping junctions contributes as much as 54% of the gene abundance. Alternative splicing may be one mechanism of regulation of the telomerase activity of TERT.

As a third example, we note that a novel exon (not in RefSeq) is observed in SALL4. Although this exon was reported in an isoform of SALL4 in Ensembl, the Ensembl-annotated isoform is a partial fragment of the IDP-predicted isoform (*SI Appendix, Fig. S11B*).

ncRNA Identification. In addition to genes coding for proteins, 480 annotated (RefSeq) multiexon ncRNAs were identified from IDP, 85% (406/480) of which are direct detections. The remaining 3,455 non-RefSeq-annotated IDP multiexon isoform predictions (green plus red plus light blue fractions in Fig. 1B: 2,103 + 325 + 1,027 = 3,455) are compared with the GENCODE lncRNA library (V12), which was created through manual curation of available cDNA and EST data. A total of 116 are found within this lncRNA library (Fig. 9A). In addition to

RefSeq and GENCODE ncRNAs, the remaining IDP isoforms were compared with the Human Body Map (HBM) long intergenic noncoding RNA (lncRNA) library, which unifies existing annotation sources with transcripts assembled from SGS RNA-Seq data collected across 24 tissues and cell types (28). Forty-six are found from this lncRNA library. To further study the remaining predictions, two functional RNA structure prediction tools, RNAz (29, 30) and alifoldz (31), were applied to predict the secondary structure potential of the novel ncRNAs remaining in the IDP output. Previous research had suggested the use of two stringency levels for predictions from two methods (32) (Fig. 9B and *SI Appendix, Methods*). To have a more confident ncRNA library for hESC study, we used a high-stringency mode for each method [$P \geq 0.9$ for RNAz; minimum free energy (MFE) ≤ -15 and Z score ≤ -4 for alifoldz]. We then took the intersection of the two sets of predictions. In total, 111 IDP novel isoforms (P value for overlap <0.0001) are predicted as structured ncRNAs by both methods. We also computed their abundance ratio in 16 human tissues with respect to H1. The abundance ratios of 104 novel ncRNAs from all 16 human tissues with respect to (w.r.t.) H1 can be computed, whereas 7 targets have insufficient short-read coverage in H1. A total of 48.08% (50/104) of novel ncRNAs have an averaged abundance ratio smaller than 0.5 with SD smaller than 0.5 (pink box in Fig. 9C), which indicates that these genes tend to have relatively higher expression in H1.

GENCODE lncRNAs and HBM lncRNAs found in hESCs have very different length distributions compared with ncRNAs predicted by our method or found in RefSeq annotations (Fig. 9D). Only 4 of the GENCODE lncRNAs (3.4%) and 1 HBM lncRNA (2.2%) are longer than 2,000 bp, whereas 216 RefSeq-annotated (45%) IDP isoforms and 72 predictions (65%) from novel IDP isoforms are longer than 2,000 bp with the averaged lengths around 2,300 bp (Table 2). Furthermore, the isoforms from the latter two IDP groups have more junctions: 183 (38%) RefSeq-annotated IDP hits and 187 predictions (70%) from novel IDP hits have more than 4 junctions (that is, at least 6 exons), whereas only 6 of GENCODE lncRNAs and none of the HBM lncRNAs have more than 4 junctions (Fig. 9E). The average number of junctions is 1.72 in the HBM lncRNA group and 1.91 in GENCODE lncRNAs, which is far smaller than 4.52 and 7.67 in the RefSeq group and IDP novel ncRNAs.

Isoforms in HBM lncRNA and GENCODE lncRNA libraries, regardless of tissue type, are generally much shorter and contain fewer junctions compared with those identified by IDP in hESCs (Fig. 9D and E). However, such striking differences are not seen in the abundance distribution (Fig. 9F). These results suggest that SGS data and manual curation of cDNA and EST data are likely to underestimate the size and complexity of ncRNA isoforms. By combining SGS and TGS data, our approach can provide a much more accurate characterization of ncRNAs. Finally, a significant percentage (27.93%, 31 of 111) of the novel

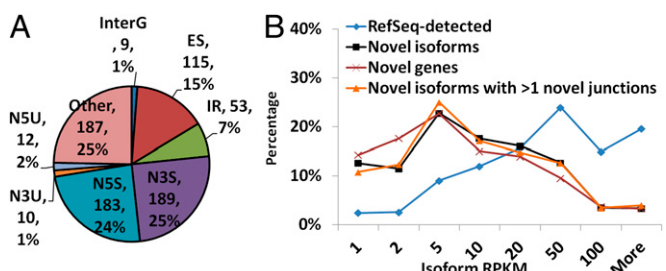
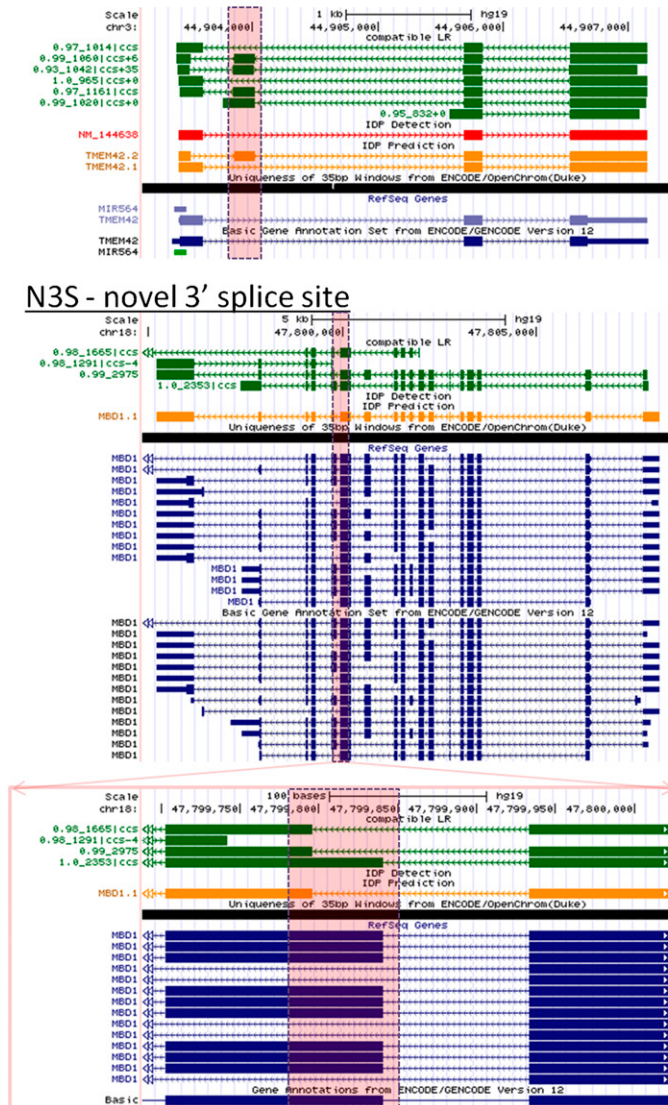
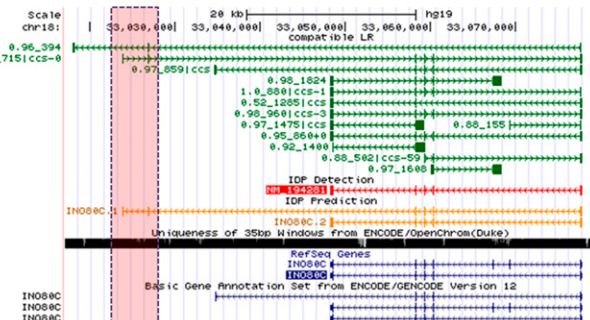


Fig. 5. Novel isoform identifications. (A) Pie chart of different novel junction types in 655 novel isoforms of existing genes. N5U, novel 5'-UTR; N3U, novel 3'-UTR; N5S, novel 5'-splice site; N3S, novel 3'-splice site; IR, intron retention; ES, exon skipping; InterG, intergenic proximal. Examples are in Fig. 6. (B) Abundance distributions of novel isoform predictions and annotated detections. Approximately 35% novel isoforms have RPKM >10 .

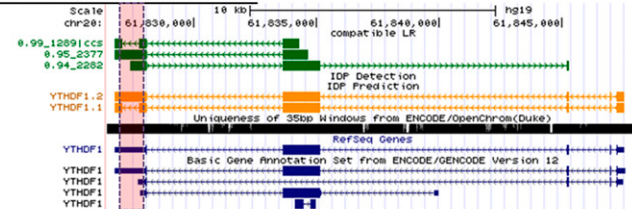
Other- novel exon



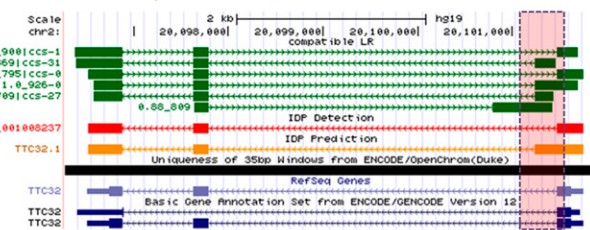
InterG – intergenic proximal



IR - intron retention



N5S - novel 5' splice site



ES - exon skipping

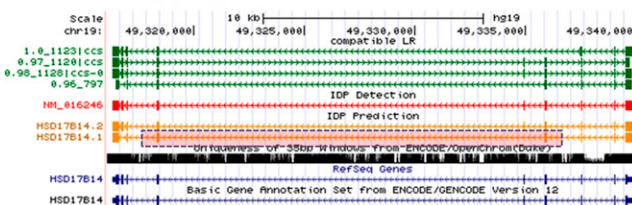


Fig. 6. Novel isoforms of existing genes with six different types of novel junctions. The genome browser setting is the same as in Fig. 2D. The GENCODE annotation is in the dark blue track. The novel junction uses are highlighted by a pink dashed box and are not reported by existing annotations but are supported by both long reads and short reads. Other: a novel exon in novel isoform TMEM142.2 is detected with two novel flanking junctions that are categorized in the “Other” group in Fig. 2C. InterG: A novel junction in novel isoform INO80C.1 is categorized as “intergenic proximal” junctions from annotated genes, but is a 3'-end junction of a novel isoform of INO80C (note that this gene is in the reverse strand). IR: A novel junction in novel isoform YTHDF1.1 indicates a splice within an annotated exon; i.e., the RefSeq annotation has a retained intron relative to YTHDF1.1. N3S: A novel junction in novel isoform MBD1.1 has a novel 3'-splice site (note that this gene is in the reverse strand). N5S: A novel junction in novel isoform TTC32.1 has a novel 5'-splice site (note that this gene is in the reverse strand). ES: Novel isoform HSD17B14.1 contains a novel junction that skips an annotated exon.

IDP lncRNA isoforms predicted by our method are highly expressed (RPKM >10, Fig. 9F). Further investigation of this set of novel, long, and highly expressed ncRNAs will be worthwhile.

Discussion

We have identified de novo isoform discovery and assembly as a fundamental obstacle to progress in RNA-Seq analysis. Innovations on both the conceptual level and the technical level are presented to overcome this obstacle. On the conceptual level, we distinguish two different types of RNA-Seq analysis and argue that it is desirable to develop different experimental and computational approaches for them separately. In discovery, analysis aims to identify all genes and gene isoforms that are being transcribed in a particular cell sample. Once it is done well for a particular species and cell type, it will contribute to the im-

provement of gene annotation for that species and will benefit all subsequent RNA analysis on that species. For quantification, on the other hand, analysis aims to estimate expression (preferably also allele-specific) levels of the gene isoforms in an annotation that specifies the set of isoforms actually present. It is anticipated that quantification analysis will be performed on a very large number of samples in translational research and in clinical applications. In these contexts it is very important to have high throughput and low cost.

A large amount of statistical and computational research has been performed over the past 5 y on how to analyze short-read RNA-Seq data for both types of analyses. It appears that many effective methods for quantification are now readily available. Most of these methods have incorporated variations of the concepts of RPKM from the Wold laboratory (1) as an expression

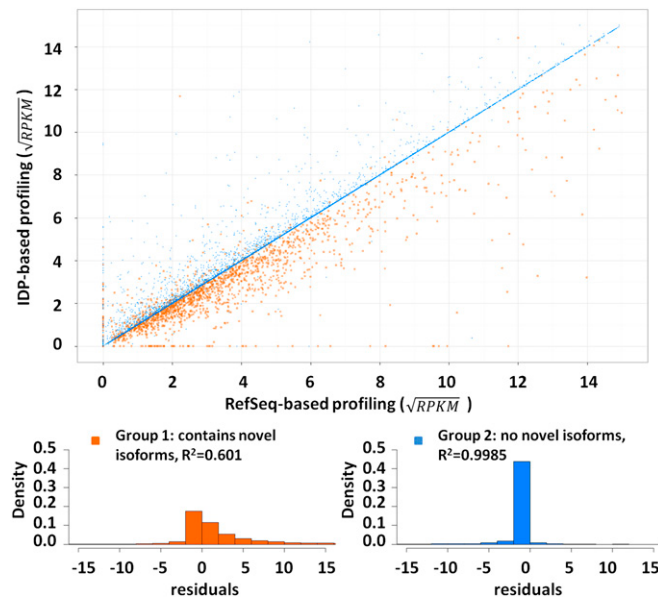


Fig. 7. Isoform abundance estimation by IDP-identified hESC transcriptome and RefSeq annotation. The gene abundances of “common isoforms” (main text) are rescaled by a square-root transformation. The genes without novel isoforms (group 2) have stable abundance estimation and have high R^2 of 0.9985 in linear regression (blue dots). In contrast, novel isoforms found in existing genes lead to a large range of abundance corrections. The residuals of linear regression show different distributions between the two groups. Group 1 (genes with novel isoforms) is highlighted in orange and group 2 in blue. The residuals of group 2 concentrate around 0, which indicates a small difference between two computations. However, group 1 has a heavy tail at the positive range. That is, most abundances of group 1 are corrected to lower values because the SGS reads must be shared with novel isoforms.

index and the Poisson deconvolution model (12) as the statistical framework for isoform-level inference. As for discovery, several algorithms, such as TopHat, SpliceMap, and MapSplice, have been developed to map splice junctions with high sensitivity and specificity. Based on the detected junctions and short-read counts, several methods such as Cufflinks and SLIDE have also been proposed to assemble the set of expressed isoforms. Our belief is that although these methods can provide useful information, the assembly problem cannot be solved effectively based on short-read RNA-Seq data alone. Instead, we pursued a hybrid TGS-

SGS sequencing approach that at this moment is more costly than SGS alone. However, the decoupling of the task of discovery from quantification allowed us to conclude that even with its higher cost, hybrid sequencing is an attractive approach for discovery, as the cost will be offset by the gained accuracy in all subsequent quantification analysis due to the resulting improvement of annotation.

On a technical level, we have developed an analysis methodology to combine the specific strengths of TGS and SGS, represented by PacBio and Illumina sequencing, respectively. Our methodology involves new statistical modeling and inference. Although the error-corrected long reads are capable of capturing many transcripts in full length, there will always be a substantial fraction of long reads that capture only partial transcript fragments. This is particularly likely if the transcript is very long. It is important to be able to combine the information from the full-length long reads and partial transcript fragment reads. Furthermore, there is also statistical information useful for isoform reconstruction, and this information can be substantial because the number of short reads will be an order of magnitude larger than the number of long reads. To effectively use all three types of reads for isoform reconstruction, we developed statistical models for how such reads are sampled from the underlying isoforms and derive appropriate algorithms to infer the isoforms based on such models. To our knowledge, such models are not available currently, and the development of these represents significant innovation in statistical methodology.

Finally, to test our method, we generated 2 million mappable long reads on H1 hESCs and analyzed them in conjunction with existing short-read RNA-Seq data. Our analysis not only illustrates the effectiveness of our method, but also provides a rich resource for stem cell biologists interested in a deeper characterization of the ESC transcriptome. Indeed, further characterization of the novel loci identified here indicates that a subset is specifically and highly expressed in pluripotent human stem cells and embryos. Moreover, silencing of these genes modulates pluripotency gene expression. Thus, at least a subset of these gene loci may have functional roles in both human development and pluripotent stem cells. Taken together, these results demonstrated the effectiveness of our methodology and suggest that gene identification, even in well-characterized cell lines and tissues, is far from complete.

Experimental Procedures

Cell Culture. Male human embryonic stem cells (H1) were used for our study. The cells were routinely cultured in feeder-free conditions on Matrigel (BD) and in mTeSR1 (Stem Cell Technologies). RNA-Seq was performed on cells between passages 50 and 55. The undifferentiated state of the hESCs was assayed by immunofluorescence for transcription factors OCT4 and NANOG

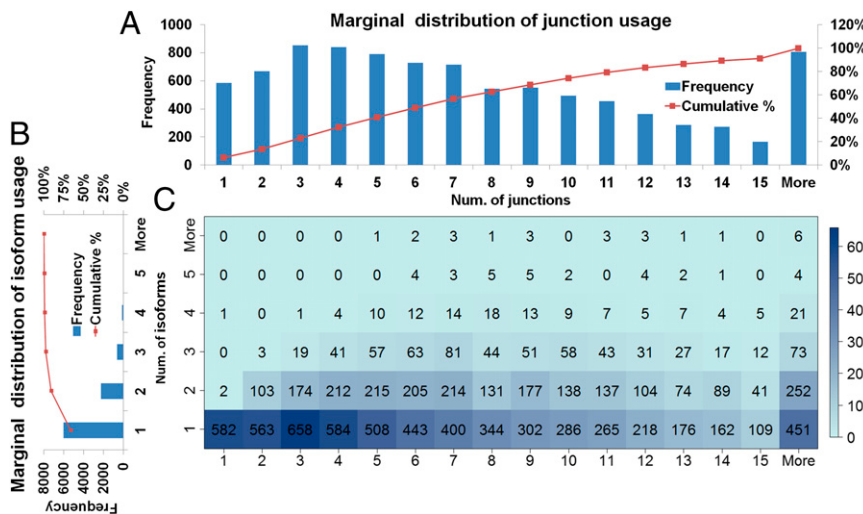


Fig. 8. (A) Marginal distributions of numbers of junction use. (B) Marginal distributions of numbers of isoform use. (C) Joint distribution displayed as heat map of number of genes by number of junctions and number of isoforms. The numbers of genes are given in each bin. Most genes express only one to two isoforms. Note that the number of junctions and the number of expressed isoforms within a gene have no significant correlation.

Table 1. Isoform identification of pluripotency markers

Pluripotency marker	RefSeq isoform identified	Novel isoforms identified
NODAL	NM_018055	
TDGF1	NM_001174136, NM_003212	
PRMT5	NM_001039619, NM_006109	
KLF4	NM_004235	
TEAD4	NM_003213, NM_201441	
E-CADHERIN	NM_004360	
LIN28A	NM_024674	
ALPL/TNAP	NM_001127501, NM_000478	
POU5F1	NM_203289, NM_002701	
NANOG	NM_024865	
DNMT3B		Novel isoforms are identified with intron retention events
ZFP42	NM_174900	A novel isoform has an alternative splicing site at the last exon
SALL4	NM_020436	A novel isoform (with 20% gene abundance) contains a novel exon
DPPA4	NM_018189	A novel isoform skips three exons
TERT		A novel isoform skips exon 7 and exon 8 and the exon-skipping junction is of high expression

and for the surface markers SSEA4, TRA-1-60, and TRA-1-81 (*SI Appendix*, Fig. S12). Pluripotency, assessed by teratoma assay, revealed the capacity of hESCs to form *in vivo* derivatives of the three germ layers (*SI Appendix*, Fig. S13).

RNA and cDNA Preparation. Total RNA was prepared by TRIzol extraction (Ambion; www.ncbi.nlm.nih.gov/pubmed/2440339) and treated with RNase-free DNase I to degrade contaminating genomic DNA. This was followed by a second extraction with acid-phenol-chloroform and the RNA was pre-

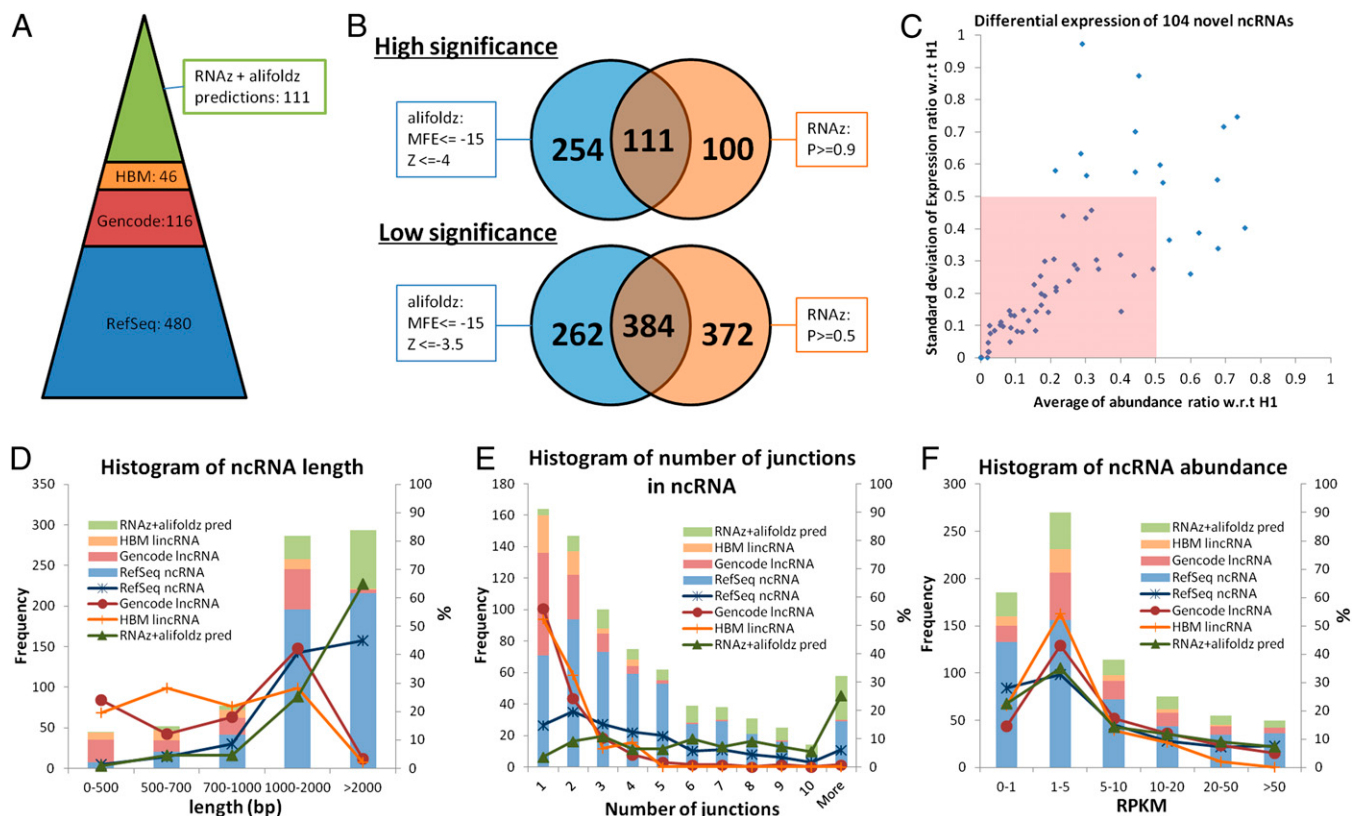


Fig. 9. Noncoding RNA identification: the distributions of length, number of junctions, and abundance. (A) Annotated ncRNA identifications and novel ncRNA predictions. A total of 480 multiexon RefSeq-annotated ncRNAs are identified from H1. After filtering out RefSeq isoforms, the remaining IDP output contains 116 GENCODE-annotated lncRNAs. After filtering out RefSeq and GENCODE isoforms, 46 HBM lncRNAs are identified. The intersection of high-significance RNAz and alifoldz predictions of the remaining novel isoforms contains 111 putative ncRNAs. (B) RNAz and alifoldz are used to identify the ncRNA from 2,428 isoform predictions. Two stringency levels are suggested by the developers. For all subsequent analyses, we use the intersection of the high-stringency outputs from the two methods as our predicted ncRNAs. (C) Differential expressions of 104 novel ncRNAs w.r.t. H1. Seven of 111 novel ncRNA predictions are not included, because of insufficient short-read coverage in H1. Fifty novel ncRNAs (inside the pink box) have an averaged abundance ratio smaller than 0.5 with SD smaller than 0.5. (D) Length distribution of IDP-identified isoforms of RefSeq ncRNA, GENCODE lncRNA, HBM lncRNA, and RNAz/alifoldz predictions. (E) Distribution of number of junctions of IDP-identified isoforms of RefSeq ncRNA, GENCODE lncRNA, HBM lncRNA, and RNAz/alifoldz predictions. (F) Abundance distribution of IDP-identified isoforms of RefSeq ncRNA, GENCODE lncRNA, HBM lncRNA, and RNAz/alifoldz predictions.

Table 2. The mean and median values of lengths, number of junctions, and abundances of four categories of ncRNAs

ncRNA Database	Length, bp	No. junctions	Abundance, RPKM
RefSeq	2,248, 1,832	4.52, 4	55.45, 3.03
GENCODE	1,012, 919	1.91, 1	10.83, 4.40
HBM	838, 832	1.72, 1	4.63, 2.27
IDP, novel ncRNA	2,402, 2,454	7.67, 7	17.97, 3.56

cipitated in 0.5 M ammonium acetate and 2.5 vol ethanol. The integrity of the RNA was tested by a Bioanalyzer RNA Nano assay (Agilent). PolyA RNA was purified from the total RNA (>100 µg), using magnetic oligo-dT beads (Dynal) according to the manufacturer's recommended protocol.

Two different manufacturer's kits and accompanying protocols for generating full-length cDNAs were used: Clontech SMARTer PCR and the Invitrogen SuperScript Full-Length cDNA kit. Each uses a retroviral reverse transcriptase to initiate cDNA synthesis at the 3' polyA tail, but the two kits use different mechanisms to capture the 5'-end information. The Clontech method relies upon template switching to an exogenous tag oligonucleotide when the reverse transcriptase reaches the 5' end of the molecule. The Invitrogen method employs an RNase I digestion and subsequent 7-methylguanosine affinity step to purify the RNA-DNA hybrids that represent a full copy of the transcript. This is followed by a DNA ligase step to add a defined sequence to the 3' ends of the full-length cDNA, before reverse transcription. For each method, 1 µg of polyA RNA served as the input material into the recommended protocol and the manufacturers' methods were followed up through second-strand cDNA synthesis. At this point, PCR (12–15 cycles; Phusion DNA polymerase; New England Biolabs) was used to amplify the double-stranded cDNA by using specific primers directed to the defined sequences present at the 5' and 3' ends of the cDNAs. Long extension times of 3.5 min ensure that longer molecules can be captured as well. The cDNA libraries were assayed by fluorimetry and Bioanalyzer assays. Both Clontech and Invitrogen kits are reproducible. For example, housekeeping genes at different sizes (ACTB, 1,808 bp; GADPH, 1,310 bp; SARS, 2,291 bp; and IARS, 2,402 bp) were purified and assayed by Bioanalyzer.

- Mortazavi A, Williams BA, McCue K, Schaeffer L, Wold B (2008) Mapping and quantifying mammalian transcriptomes by RNA-Seq. *Nat Methods* 5(7):621–628.
- Wang Z, Gerstein M, Snyder M (2009) RNA-Seq: A revolutionary tool for transcriptomics. *Nat Rev Genet* 10(1):57–63.
- Ingolia NT, Ghaemmaghami S, Newman JRS, Weissman JS (2009) Genome-wide analysis in vivo of translation with nucleotide resolution using ribosome profiling. *Science* 324(5924):218–223.
- Mitchell JA, et al. (2012) Nuclear RNA sequencing of the mouse erythroid cell transcriptome. *PLoS ONE* 7(11):e49274.
- Li M, et al. (2011) Widespread RNA and DNA sequence differences in the human transcriptome. *Science* 333(6038):53–58.
- Rederstorff M, et al. (2010) RNomics: Defining the ncRNA transcriptome by cDNA library generation from ribonucleo-protein particles. *Nucleic Acids Res* 38(10):e113.
- Licalatosi DD, et al. (2008) HITS-CLIP yields genome-wide insights into brain alternative RNA processing. *Nature* 456(7221):464–469.
- Chi SW, Zang JB, Mele A, Darnell RB (2009) Argonaute HITS-CLIP decodes microRNA-mRNA interaction maps. *Nature* 460(7254):479–486.
- Au KF, Jiang H, Lin L, Xing Y, Wong WH (2010) Detection of splice junctions from paired-end RNA-seq data by SpliceMap. *Nucleic Acids Res* 38(14):4570–4578.
- Trapnell C, Pachter L, Salzberg SL (2009) TopHat: Discovering splice junctions with RNA-Seq. *Bioinformatics* 25(9):1105–1111.
- Wang K, et al. (2010) MapSplice: Accurate mapping of RNA-seq reads for splice junction discovery. *Nucleic Acids Res* 38(18):e178.
- Jiang H, Wong WH (2009) Statistical inferences for isoform expression in RNA-Seq. *Bioinformatics* 25(8):1026–1032.
- Hiller D, Jiang H, Xu W, Wong WH (2009) Identifiability of isoform deconvolution from junction arrays and RNA-Seq. *Bioinformatics* 25(23):3056–3059.
- Trapnell C, et al. (2010) Transcript assembly and quantification by RNA-Seq reveals unannotated transcripts and isoform switching during cell differentiation. *Nat Biotechnol* 28(5):511–515.
- Li JJ, Jiang C-R, Brown BJ, Huang H, Bickel PJ (2011) Sparse linear modeling of RNA-seq data for isoform discovery and abundance estimation. *Proc Natl Acad Sci USA* 108: 19867–19872.
- Hiller D, Wong WH (2013) Simultaneous isoform discovery and quantification from RNA-seq. *Stat Biosci* 5(1):100–118.
- Pruitt KD, Tatusova T, Brown GR, Maglott DR (2012) NCBI Reference Sequences (RefSeq): Current status, new features and genome annotation policy. *Nucleic Acids Res* 40 (Database issue):D130–D135.
- English AC, et al. (2012) Mind the gap: Upgrading genomes with Pacific Biosciences RS long-read sequencing technology. *PLoS ONE* 7(11):e47768.
- Au KF, Underwood JG, Lee L, Wong WH (2012) Improving PacBio long read accuracy by short read alignment. *PLoS ONE* 7(10):e46679.
- Miura T, et al. (2004) Monitoring early differentiation events in human embryonic stem cells by massively parallel signature sequencing and expressed sequence tag scan. *Stem Cells Dev* 13(6):694–715.
- Harrow J, et al. (2006) GENCODE: Producing a reference annotation for ENCODE. *Genome Biol* 7(Suppl 1):S4:1–9.
- Bernstein BE, et al.; ENCODE Project Consortium (2012) An integrated encyclopedia of DNA elements in the human genome. *Nature* 489(7414):57–74.
- Djebali S, et al. (2012) Landscape of transcription in human cells. *Nature* 489(7414): 101–108.
- Flicek P, et al. (2011) Ensembl 2011. *Nucleic Acids Res* 39(Database issue):D800–D806.
- Hsu F, et al. (2006) The UCSC known genes. *Bioinformatics* 22(9):1036–1046.
- Adams MD, Soares MB, Kerlavage AR, Fields C, Venter JC (1993) Rapid cDNA sequencing (expressed sequence tags) from a directionally cloned human infant brain cDNA library. *Nat Genet* 4(4):373–380.
- Derrien T, et al. (2012) The GENCODE v7 catalog of human long noncoding RNAs: Analysis of their gene structure, evolution, and expression. *Genome Res* 22(9): 1775–1789.
- Cabili MN, et al. (2011) Integrative annotation of human large intergenic noncoding RNAs reveals global properties and specific subclasses. *Genes Dev* 25(18):1915–1927.
- Washietl S, Hofacker IL, Stadler PF (2005) Fast and reliable prediction of noncoding RNAs. *Proc Natl Acad Sci USA* 102(7):2454–2459.
- Gruber AR, Findeiß S, Washietl S, Hofacker IL, Stadler PF (2010) RNAz 2.0: Improved noncoding RNA detection. *Pac Symp Biocomput* 15:69–79.
- Washietl S, Hofacker IL (2004) Consensus folding of aligned sequences as a new measure for the detection of functional RNAs by comparative genomics. *J Mol Biol* 342(1):19–30.
- Washietl S, et al. (2007) Structured RNAs in the ENCODE selected regions of the human genome. *Genome Res* 17(6):852–864.

NM_002161, 4,406 bp and NM_013417, 4,510 bp) are detected by full-length long reads from the two preparations (*SI Appendix, Figs. S14–S17*).

Size selection was used with each of the cDNA libraries to enrich for larger cDNA molecules. Briefly, 500 ng of double-stranded cDNA was separated on a 1x TAE agarose gel and stained with SybrSafe. The gel was visualized on blue light to avoid DNA damage and, using a size standard in a parallel lane, size fractions were cut from the gel from 1 kb to 2 kb, from 2 kb to 3 kb, and from 3 kb to 10 kb. The DNA was recovered from each fraction, using a silica column kit (Zymo), and the DNA was then subjected to additional PCR to enrich for molecules in each size fraction. For both non-size-selected and size-selected PCR reactions, the double-stranded cDNA was purified via AMPure PB beads (Pacific Biosciences), using a 0.5x ratio of bead slurry to PCR.

Single-Molecule Sequencing. Sequencing templates were prepared using the manufacturer's SMRTbell template protocol (Pacific Biosciences Large Template Prep kit), with a minimum of 1 µg of dsDNA input into each library procedure. After exonuclease digestion of incomplete SMRTbell templates, the libraries were purified by three sequential 0.5x AMPure PB purifications (Pacific Biosciences.) Libraries were quantified by fluorimetry and assayed for quantity and size distribution by Bioanalyzer. Sequencing was performed on the Pacific Biosciences RS, using standard protocols for C2 chemistry with the C2 or XL enzyme.

ACKNOWLEDGMENTS. We thank Dr. Arnold Ludwig Hayer, Dr. Tobias Meyer, Dr. Laughing Bear Torrez, and Dr. Diana Cepeda for help in designing siRNA experiments and for technical help in performing the knockdown experiments. K.F.A. and W.H.W. were supported by the National Human Genome Research Institute (R01HG005717). B.A.W. was partially supported by the California Institute of Technology Beckman Center for Functional Genomics. The Illumina short-read data were generated as part of the Encode project (National Human Genome Research Institute Grants U54 HG004576 and U54 HG006998 to Barbara Wold). V.S., J.D.D., and R.A.R.-P. were supported by the National Heart, Lung, and Blood Institute (U01HL100397) and the National Institute of Child Health and Human Development (U54 HD068158).

METHODS

Short reads alignment and exon junction detections by SpliceMap

SpliceMap 3.3.6 was used to align 113 million (pairs of) 100bp paired-end reads (226 million reads) to the reference human genome (hg19). Maximum intron size was set at 400,000 and the lower 25th-percentile intron size was set at 20,000. Maximum number of multi-hits was 10. Maximum number of mismatches allowed in seeding for junction search was 2 and maximum number of mismatches allowed in entire read was 4. Bowtie 0.12.7 [32] was the initial aligner in SpliceMap and "try_hard" option was used. In this way, we found 116 million reads mappable to reference genome hg19.

To find candidates of novel gene loci, we identify clusters of novel junctions. Define the distance between two junctions as the minimum length between either splice sites of each junction. Any two novel junctions that are separated by less than 2,000bp are clustered together. In this way, 2,568 clusters of novel junctions are found from H1 junction detections.

Error correction of PacBio long reads by LSC

The accuracy of PacBio long reads is generally not as high as SGS short reads. We have previously developed a method (LSC, ref[18]) to correct errors of PacBio reads by alignment with SGS short reads. LSC 0.2.2 was used to correct PacBio subreads and CCS reads. The options "l_nonredundant" and "l_RemoveBothTails" were set to "Y". The length of pseudo chromosomes was 50,000,000 and the length of gap sequence between long reads was 100. Minimum number of non'N' after compressing was set to 39 and "maximum 'N' are allowed after compressing" was 1.

IDP - Isoform Detection and Prediction

IDP (<http://www.stanford.edu/~kinfai/IDP/IDP.html>) uses long read and junctions as input. Error-corrected long reads are used (Figure S1). The junction linkages within a long reads is defined by the BLAT alignment on reference genome. Subsequently, they are compared with reference annotation library such as RefSeq to find the detections of annotated isoforms. Long reads are filtered out if any junctions are not supported by junction detections or reference annotations. Shorter redundant long reads are then excluded and the isoform candidate construction is based on the remaining nonredundant long reads. Relative abundance estimated from short read coverage is used to select isoforms. Each steps are described with more details in the following subsections.

Error-corrected long read alignment, junction linkage definition and isoform detection

BLAT is used to align LSC-corrected long reads to the reference human genome (hg19). The alignment with highest identity (number of mismatches/full length) of each long read was selected. Since 99% of the shortest junctions from genes are longer than 68bp (Figure S2), the alignment gaps longer than 68bp are defined as splices. The strand of gene structure of a long reads is defined by the strands of its junctions. If the junction set of an annotated isoform has identical detection sets from long reads, this annotated isoform is regarded as a detection.

Gene locus definition and exon boundary definition

IDP uses the gene loci in RefSeq annotation as the initial seeds of gene locus definition. The gene isoform loci are merged, if there are overlaps between them. Subsequently, the novel junction detections from SpliceMap extend the gene loci if there are overlaps. If a novel junction spans more than a certain number of the reference gene loci, it is filtered out from this gene loci extension. In the hESC study, we set this number to 1.

Next, we define exon boundaries within each gene locus. Two types of boundaries are included: 1) all splice sites of novel junctions and annotated junctions. 2) 5' and 3'ends of all annotated gene isoforms. Two flanking bases around exon boundary Pi are labeled as Pi- and Pi+ (Figure S3A).

Nonredundant long read selection

Since the number of long reads is large, there exist many redundant reads. We first remove this redundancy, in order to produce a set of nonredundant reads. According to the exon boundary definition, gene structures can be denoted by an ordered set of exon boundaries (Figure S3B). The exon boundaries that are covered by a long read is included in its ordered set for definition of gene structure. If gene structures of two long reads are identical, then they contain redundant information for the definition of the gene locus, and the shorter one is filtered out. If the gene structure of a long reads is a proper subset of the other, then it is also redundant and is filtered out. After filtering, a set of 60,387 nonredundant long reads are retained and used for isoform candidate construction.

Isoform candidate construction

Long read data was generated from polyT selected RNA libraries. Thus, initial 3'ends are defined by the detections of polyA or polyT and the corresponding primers that are next to them. The closest

downstream exon boundary of each initial 3'end is defined as the potential 3'end for the following isoform construction. All annotated 5' and 3' ends are included as potential ends as well. CAGE data is optional to for definition of potential 5' end. However, the FPR is not low enough for the ENCODE CAGE data and will lower the specificity of IDP output in this hESC research. Therefore, ENCODE CAGE data was not used in this study.

Annotated junctions and reliable novel junction detections (with nNR > 1, see ref [9]) are used for the following isoform construction. For each nonredundant long read within a gene locus, upstream and downstream junctions with the same strand as long read are added to fill the gap between 3' and 5'ends of the long read and all potential 5' and 3' ends of the gene locus. If there are no potential 5' or 3' ends defined in a gene locus, all possible combinations of junctions are included in candidate pool and set the first or the last exon length to 200bp (Figure S4). Isoform candidates that have exon longer than 1,700bp are excluded, because 96.48% of reference exons are shorter than 1,700bp (Figure S5). To avoid too many isoform constructions from very short fragments, isoform construction is not performed if there are more than 10 junctions between nonredundant long read and the potential ends. In addition, gene locus with more than 50 isoform candidates is also excluded so that the computational intensity of the MAP (Maximum A Posterior) is reasonable (Figure S6). These conditions resulted in the exclusion of about 10% of the loci from subsequent annotation.

Abundance estimation by MAP (Maximum A Posterior) and isoform selection

Jiang and Wong [11] proposed a Poisson model of counting the observed short reads (SR) to estimate isoform abundance (Figure S7). With the same model setting, we have the likelihood function:

$$P(\{X_s = x_s, s \in S\} | \Theta) = \prod_s P(X_s = x_s | \Theta) = \prod_s \frac{e^{-\lambda_s} \lambda_s^{x_s}}{x_s!}$$

Where X_s is the number of reads mapped to region s (exonic or junction region)

S is the set of all indexed regions.

H is the set of all isoforms.

$\Theta = \{\theta_h\}_1^H$ are the expression levels of the set of isoforms H

$\lambda_s = N l_s \sum_h^H c_{sh} \theta_h$ and c_{sh} is the indicator of whether isoform h contains region s

l_s is the length of region s .

N is the total number of mappable SRs.

Instead of solving Θ by maximizing the likelihood function, based on experimental evidence we developed an informative prior for the expression parameter Θ (see the "Experimental prior of isoform abundance") and maximize the corresponding posterior density to obtain the MAP estimate for Θ .

Specifically, the posterior function is given by:

$$P(\Theta | \{X_s = x_s, s \in S\}) \propto P(\{X_s = x_s, s \in S\} | \Theta) P(\Theta | I_{Detection})$$

where $P(\Theta | I_{Detection}) = \prod_h P(\theta_h | I_{Detection})$, and $P(\theta_h | I_{Detection})$ is the conditional density of θ_h given either 1) isoform h is detected by error-corrected PacBio long reads ($I_{Detection} = 1$) or 2) not detected by error-corrected PacBio long reads ($I_{Detection} = 0$)

Taking logarithm on the above equation, we have:

$$\sum_s -\lambda_s + x_s \log \lambda_s - \log(x_s!) + \sum_h \log(P(\theta_h | I_{Detection}))$$

That is, we need to maximize

$$\sum_s -\lambda_s + x_s \log \lambda_s + \sum_h \log(P(\theta_h | I_{Detection}))$$

subject to $\lambda_s = N l_s \sum_h c_{sh} \theta_h$ and $\theta_h > 0$

As shown in "Experimental prior of isoform abundance", we approximate $\log(P(\theta_h | I_{Detection}))$ as linear function of θ_h . Since Jiang and Wong (2009) have already shown that $\sum_s -\lambda_s + x_s \log \lambda_s$ is concave and $\log(P(\theta_h | I_{Detection}))$ is linear (see "Experimental prior of isoform abundance"), the log-posterior density is thus concave in Θ . We apply hill-climbing algorithm to optimize it.

In a given gene locus, the relative abundance of each isoform is defined as its abundance divided by the sum of all isoform abundances in this gene locus. A relative abundance threshold is used to select isoforms predictions at a given FPR threshold (see ROC analysis). In this hESC data, we selected the isoform candidates with relative abundance larger than 16.27%, which corresponds to a FPR of 0.05 in the ROC curve.

Experimental prior of isoform abundance

We use the following prior for isoform candidate that is detected directly from long reads:

$$P(\theta | I_{Detection} = 1) = \frac{1}{\theta_{max}}$$

where θ_{max} is a the upper bound of possible gene abundances and set to a large constant value.

Given the length, Isoform with higher expression level is more likely to be detected directly. Therefore, the undetection rate of annotated isoform with respect to the abundance θ could be an approximate of the prior of isoform candidates that are not detected:

If an isoform with length L exists in the sample:

$$P(\theta | I_{Detection} = 0) = P(I_{Detection} = 0 | \theta) \frac{P(\theta)}{P(I_{Detection} = 0)}$$

where $P(I_{Detection} = 0 | \theta)$ is the undetection rate w.r.t isoform abundance θ . Given no preference of $P(\theta)$, we have:

$$P(\theta | I_{Detection} = 0) \propto P(I_{Detection} = 0 | \theta)$$

According the experimental data, we assume $P(I_{Detection} = 0 | \theta) = \exp(\beta(L)\theta) / C(L)$ where L is the isoform length and C is a normalization constant. In order to estimate $\beta(L)$, 500 annotated isoforms whose sizes are closest to L are divided into five length bins. Within each bin, logarithm of undetection rate by long read data and the median RPKM estimated by rSeq [11] are calculated. Then, a linear regression of these five data points are performed, where the linear coefficient is the estimate of $\beta(L)$. Plugging it in the target function, we have:

$$\sum_s -\lambda_s + x_s \log \lambda_s + \sum_h \beta(L_h) \theta_h$$

Definition of false and true positives

A library of two-consecutive-junction linkages (TCJL) is generated from RefSeq, Ensembl, Gencode, KnownGene and EST (Figure S8). These reference libraries are based on hundreds of thousands of data from different samples, different techniques and different research groups. Although some data may only cover fragments of transcripts, most possible linkages of two consecutive junctions in nature are likely to be seen in these libraries. Thus, we regard an isoform candidate as false positive if any two-consecutive-junction linkage of this isoform is not supported by TCJL. On the other hand, we regard isoform candidates as true isoforms if they are directly detected. Relative abundance (isoform abundance/gene abundance) is the classifier parameter to control FPR of the IDP output (Figure 1C). FPR is computed from (number of false positive isoform prediction/number of isoform predictions) and sensitivity is (number of true positive isoform predictions/number of true isoforms)

ROC analysis

In order to compare IDP and Cufflinks 1.1.0, we use one half of PacBio long reads to find the full-length detections of RefSeq annotated isoforms, which are regarded as the gold standard (true positive) library. Then, we run IDP with the other half of long reads and run cufflinks with the short reads. The definition of "false positive" isoforms are the same as the previous subsection. Using relative abundance as the classifier parameter, then we filter outputs from two tools and calculate sensitivities and FPRs.

ncRNA prediction by RNAz and Alifoldz

Two programs, RNAz [28][29] and alifoldz [30] were used to detect functional RNA structures among the novel detected isoform predictions. Alifoldz finds stable RNA-secondary structures by comparing the consensus minimum free energy (MFE) with respect to a number of randomized alignments. The normalized z-score is computed as $z = (m - \mu)/\sigma$, where m is MFE of native RNA, μ is the mean and σ is the standard deviation of random RNAs MFEs. It indicates the stability of RNA structure with respect to random alignments. RNAz uses two metrics 1) thermodynamic stability, which is measured for each alignment sequence and the average is reported as z-score, 2) conservation of secondary structure, computed as the consensus MFE to the average MFE of each sequence, reported as structural conservation index (SCI).

In order to provide the required multiple sequence alignment as input, we used "Multiple alignments of 45 vertebrate genomes with Human" from UCSC browser [33] and extracted and concatenated alignment blocks corresponding to each transcript region. RNAz does not accept alignments longer than 400 columns, so we used rnazWindow.pl program to pre-process the alignments. We used up to six sequences with window size of 120, slide 40 and minimum four sequences as suggested in RNAz manual. The same window size and slide of 120 and 40 are also used for alifoldz and up to 10 sequences in the alignment blocks with minimum 4 sequences were retained which had at least 60% mean pairwise identity. There are two thresholds suggested by RNAz for its computed SVM RNA-class probability: 0.5 and a more stringent threshold of 0.9. For alifoldz we used two z-score cutoff thresholds -3.5 and -4 for alignments with consensus MFE < -15. Transcript sequences which had a hit within the above-mentioned thresholds are considered as potential ncRNA candidates.

Gene expression analysis

Gene expression analysis was performed using Fluidigm (San Francisco, CA) analysis and following the protocol "Single-Cell Gene Expression Using EvaGreen DNA Binding Dye". Briefly, purchased forward and reverse primer pairs were mixed together to a final concentration of 20 μ M. All primer pairs were pooled together at a final concentration of 200nM each for pre-amplification.

CellsDirect 2x Reaction Mix (Invitrogen), SuperScript III RT Platinum Taq Mix (Invitrogen), 4X Primer Mix (200 nM) and TE buffer were prepared at total volume of 9 μ l. Cells (10-200) were manually picked under the dissection hood added in 1 μ l to each reaction and the following thermal cycling protocol was set: Reverse Transcription - 50°C for 15 min, Inactivate RT/Activate Taq - 95°C for 2 min, 18 Cycles - 95°C for 15 sec and 60°C for 4 min, 4°C for infinite. ExoSAP-IT treatment removed unused material and was performed at 37°C for 15 min (Digest) and 80°C for 15 min (Inactivation). Reaction was diluted 1:5 in TE buffer and stored at -20°C or immediately used for Sample Pre-Mix. Sample Pre-Mix, Samples and Assay Mix was prepared according to the protocol. The Fluidigm chip was primed and loaded with the assay and sample mix. Data were collected and analyzed using the Fluidigm Data Collection Software v.3.0.2.

mRNA transfection

mRNA transfection was carried out with RNAiMAX (Invitrogen) according to the manufacturer's instruction in a 6well format. Briefly, RNA and reagent were first diluted in Opti-MEM basal medium (Invitrogen). 1.2 ug (100 ng/ μ l) RNA was diluted in 48ul Opti-MEM and 6ul RNAiMAX was diluted in 54 ul Opti-MEM. Both dilutions were combined to a total of 120ul, briefly vortexed and incubated for 15 min at room temperature. After complex formation, mix was drop-wise dispensed to culture medium. RNA transfection was performed in Pluriton media (Stemgent) supplemented with Pluriton supplement (Stemgent) and B18R interferon inhibitor (eBioscience) at 200 ng/ml.

Derivation of mRNA induced pluripotent stem cells (RiPSCs)

Target fibroblasts were seeded at 1x10⁴-5x10⁴ cells per well of a 6-well plate on 0.2% gelatin coated wells and cultured in Pluriton media. After 24 hours, Pluriton media was changed to NuFF (Globalstem) conditioned Pluriton media (Stemgent) supplemented with Pluriton supplement (Stemgent) and B18R (200 ng/ml, eBioscience). Cells were transferred to a low oxygen environment (5%) for higher reprogramming efficiencies before the first transfection. After 2 hrs of equilibration in low oxygen conditions the mRNA cocktail containing OSKMLg (*OCT3/4*, *SOX2*, *KLF4*, *cMYC*, *LIN28A*, *eGFP*) was transfected and repeated every 24h until colony formation was observed. Incubation of mRNA and transfection mix with cells was carried out for 4h. Media was replaced with fresh Pluriton media (Stemgent) containing Pluriton supplement and B18R recombinant protein (200ng/ml) to inhibit cellular immune response.

Primary colonies were picked onto fresh culture dishes coated with Matrigel (BD Bioscience) and media was replaced with mTeSR1 (STEMCELL Technologies) supplemented with 5X mTeSR1 supplement (STEMCELL Technologies) and Nutristem (Stemgent). Established iPSCs lines were cultured under 20% oxygen conditions.

REFERENCES

- [1] Mortazavi, A., Williams, B.A., McCue, K., Schaeffer, L., Wold, B. (2008) Mapping and quantifying mammalian transcriptomes by RNA-Seq. *Nat Methods.* 5, 621-628.
- [2] Wang, Z., Gerstein, M., Snyder, M. (2009) RNA-Seq: a revolutionary tool for transcriptomics. *Nat Rev Genet.* 10, 57-63.
- [3] Ingolia, N.T., Ghaemmaghami, S., Newman, J.R.S., Weissman, J.S. (2009) Genome-Wide Analysis in Vivo of Translation with Nucleotide Resolution Using Ribosome Profiling. *Science* 324, 218–223.
- [4] Mitchell, J.A., Clay, I., Umlauf, D., Chen, C.Y., Moir, C.A., Eskiw, C.H., Schoenfelder, S., Chakalova, L., Nagano, T., Fraser, P. (2012) Nuclear RNA Sequencing of the Mouse Erythroid Cell Transcriptome. *PLoS ONE* 7, e49274.
- [5] Li, M., Wang, I.X., Li, Y., Bruzel, A., Richards, A.L., Toung, J.M., Cheung, V.G. (2011) Widespread RNA and DNA Sequence Differences in the Human Transcriptome. *Science* 333, 53-58.
- [6] Rederstorff, M., Bernhart, S.H., Tanzer, A., Zywicki, M., Perfler, K., Lukasser, M., Hofacker, I.L., Huttenhofer, A. (2010) cDNA library generation from ribonucleo-protein particles. *Nucleic Acids Res.* 38, e113.
- [7] Licatalosi, D.D., Mele, A., Fak, J.J., Ule, J., Kayikci, M., Chi, S.W., Clark, T.A., Schweitzer, A.C., Blume, J.E., Wang, X., Darnell, J.C., Darnell, R.B. (2008) HITS-CLIP yields genome-wide insights into brain alternative RNA processing. *Nature* 456, 464-469.
- [8] Chi, S.W., Zang, J.B., Mele, A., Darnell, R.B. (2009) Argonaute HITS-CLIP decodes microRNA–mRNA interaction maps. *Nature* 460, 479-486
- [9] Au, K.F., Jiang, H., Lin, L., Xing, Y., Wong, W.H. (2010) Detection of splice junctions from paired-end RNA-seq data by SpliceMap. *Nucleic Acids Res.* 38, 4570-4578.
- [10] Trapnell, C., Pachter, L., Salzberg, S.L. (2009) TopHat: discovering splice junctions with RNA-Seq. *Bioinformatics* 25, 1105-1111.

- [11] Wang, K., Singh, D., Zeng, Z., Coleman, S.J., Huang, Y., Savich, G.L., He, X., Mieczkowski, P., Grimm, S.A., Perou, C.M., et al. (2010) MapSplice: accurate mapping of RNA-seq reads for splice junction discovery. *Nucleic Acids Res.* 38, e178.
- [12] Jiang, H., Wong, W. H. (2009) Statistical Inferences for Isoform Expression in RNA-Seq. *Bioinformatics* 25, 1026–1032
- [13] Hiller, D., Jiang, H., Xu, W., Wong, W.H. (2009) Identifiability of isoform deconvolution from junction arrays and RNA-Seq. *Bioinformatics* 25, 3056-3059
- [14] Trapnell, C., Williams, B.A., Pertea, G., Mortazavi, A., Kwan, G., van Baren, M.J., Salzberg, S.L., Wold, B.J., Pachter, L. (2010) Transcript assembly and quantification by RNA-Seq reveals unannotated transcripts and isoform switching during cell differentiation. *Nat Biotechnol.* 28, 511-515.
- [15] Li, J.J., Jiang, C-R., Brown, B.J., Huang, H., Bickel, P.J. (2011) Sparse linear modeling of RNA-seq data for isoform discovery and abundance estimation. *Proc. Natl. Acad. Sci. U.S.A.* 108, 19867-19872
- [16] Hiller, D., Wong, W.H. (2012) Simultaneous isoform discovery and quantification from RNA-seq. *Stat Biosci.* 5, 100-118
- [17] Pruitt, K.D., Tatusova, T., Brown, G.R., Maglott, D.R. (2012) NCBI Reference Sequences (RefSeq): current status, new features and genome annotation policy. *Nucleic Acids Res.* 40(Database issue), D130-135.
- [18] English, A.C., Richards, S., Han, Y., Wang, M., Vee, V., Qu, J., Qin, X., Muzny, D.M., Reid, J.G., Worley, K.C., Gibbs, R.A. (2012) Mind the gap: upgrading genomes with Pacific Biosciences RS long-read sequencing technology. *PLoS One.* 7, e47768.
- [19] Au, K.F., Underwood, J.G., Lee, L., Wong, W.H. (2012) Improving PacBio long read accuracy by short read alignment. *PLoS One* 10, e46679.
- [20] Miura, T., Luo, Y., Khrebtukova, I., Brandenberger, R., Zhou, D., Thies, R.S., Vasicek, T., Young, H., Lebkowski, J., Carpenter, M.K., Rao, M.S. (2004) Monitoring early differentiation events in human

embryonic stem cells by massively parallel signature sequencing and expressed sequence tag scan.
Stem Cells Dev. 13, 694-715

[21] Harrow, J., Denoeud, F., Frankish, A., Reymond, A., Chen, C.K., Chrast, J., Lagarde, J., Gilbert, J.G., Storey, R., Swarbreck, D., et al. (2006) GENCODE: producing a reference annotation for ENCODE. Genome Biol. 7, Suppl 1:S4.1-9.

[22] The ENCODE Project Consortium. (2012) An integrated encyclopedia of DNA elements in the human genome. Nature 489, 57-74.

[23] Djebali, S., Davis, C.A., Merkel, A., Dobin, A., Lassmann, T., Mortazavi, A., Tanzer, A., Lagarde, J., Lin, W., Schlesinger, F. et al. (2012) Landscape of transcription in human cells. Nature 489, 101-108

[24] Flicek, P., Amode, M.R., Barrell, D., Beal, K., Brent, S., Chen, Y., Clapham, P., Coates, G., Fairley, S., Fitzgerald, S., et al. (2011) Ensembl 2011. Nucleic Acids Res. 39 (Database issue), D800-806.

[25] Hsu, F., Kent, W.J., Clawson, H., Kuhn, R.M., Diekhans, M., Haussler, D. (2006) The UCSC known genes. Bioinformatics 22, 1036–1046.

[26] Adams, M.D., Soares, M.B., Kerlavage, A.R., Fields, C., Venter, J.C. (1993) Rapid cDNA sequencing (expressed sequence tags) from a directionally cloned human infant brain cDNA library. Nat. Genet. 4, 373–380.

[27] Derrien, T., Johnson, R., Bussotti, G., Tanzer, A., Djebali, S., Tilgner, H., Guernec, G., Martin, D., Merkel, A., Knowles, D.G., et al. (2012) The GENCODE v7 catalog of human long noncoding RNAs: analysis of their gene structure, evolution, and expression. Genome Res. 22, 1775-1789.

[28] Cabili, M.N., Trapnell, C., Goff, L., Koziol, M., Tazon-Vega, B., Regev, A., Rinn, J.L. (2011) Integrative annotation of human large intergenic noncoding RNAs reveals global properties and specific subclasses. Genes Dev. 25, 1915-1927.

[29] Washietl S., Hofacker I.L., Stadler P.F. (2005) Fast and reliable prediction of noncoding RNAs Proc. Natl. Acad. Sci. U.S.A. 102, 2454-2459.

- [30] Gruber, A.R., Findeiß, S., Washietl, S., Hofacker, I.L., Stadler, P.F. (2010) RNAz 2.0: Improved noncoding RNA detection. Pac Symp Biocomput. 15, 69-79
- [31] Washietl, S., Hofacker, I.L. (2004) Consensus folding of aligned sequences as a new measure for the detection of functional RNAs by comparative genomics. J. Mol. Biol. 342, 19-30.
- [32] Washietl, S., Pedersen, J.S., Korbel, J.O., Stocsits, C., Gruber, A.R., Hackermüller, J., Hertel, J., Lindemeyer, M., Reiche, K., Tanzer, A., et al. (2007) Structured RNAs in the ENCODE selected regions of the human genome. Genome Res. 17, 852-864.
- [33] Langmead, B., Trapnell, C., Pop, M., Salzberg, S.L. (2009) Ultrafast and memory-efficient alignment of short DNA sequences to the human genome. Genome Biol. 10, R25.
- [34] UCSC Genome Browser (2013) <http://hgdownload.cse.ucsc.edu/downloads.html> Accessed 10/31/2013

SUPPLEMENTARY FIGURES

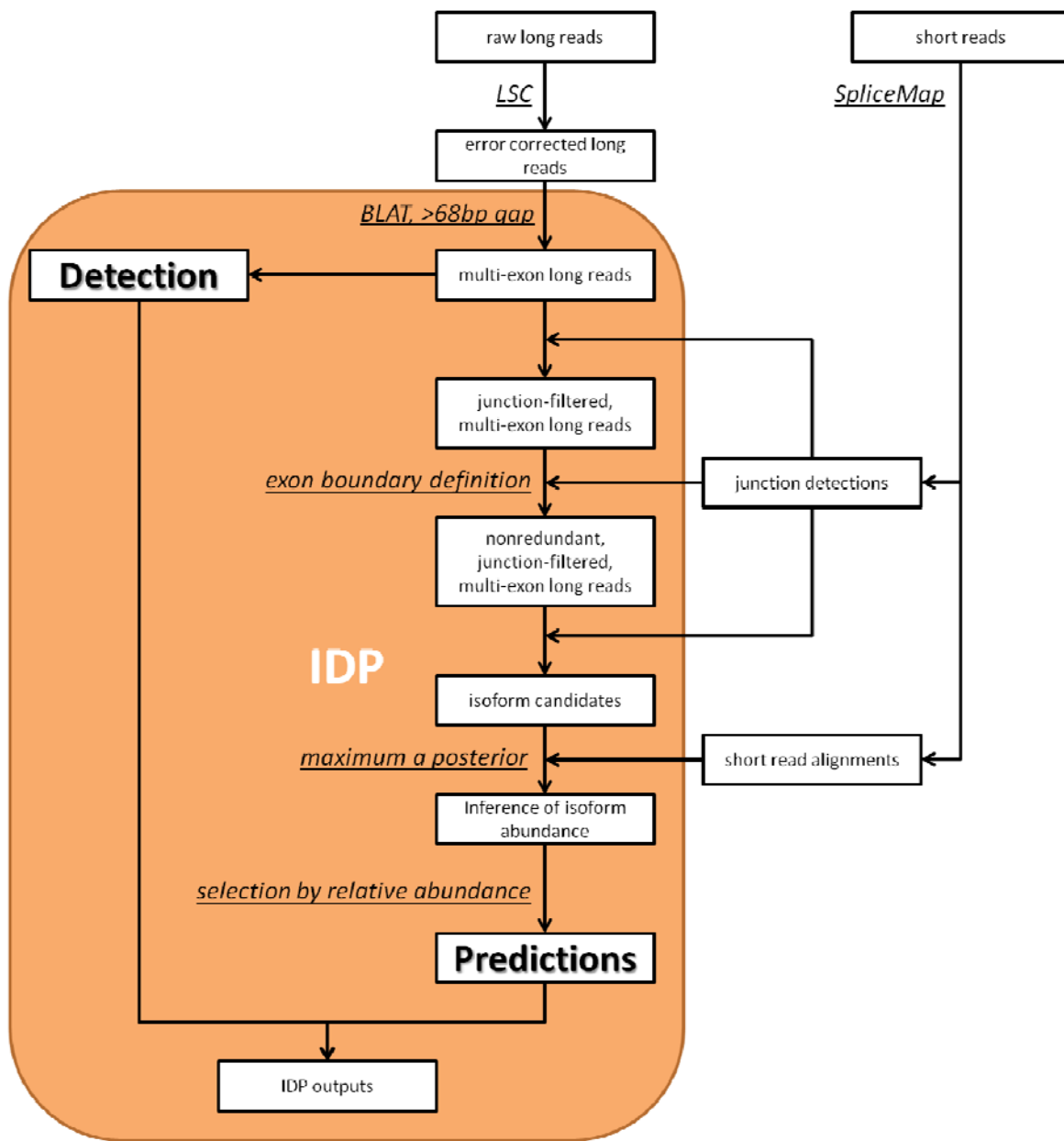
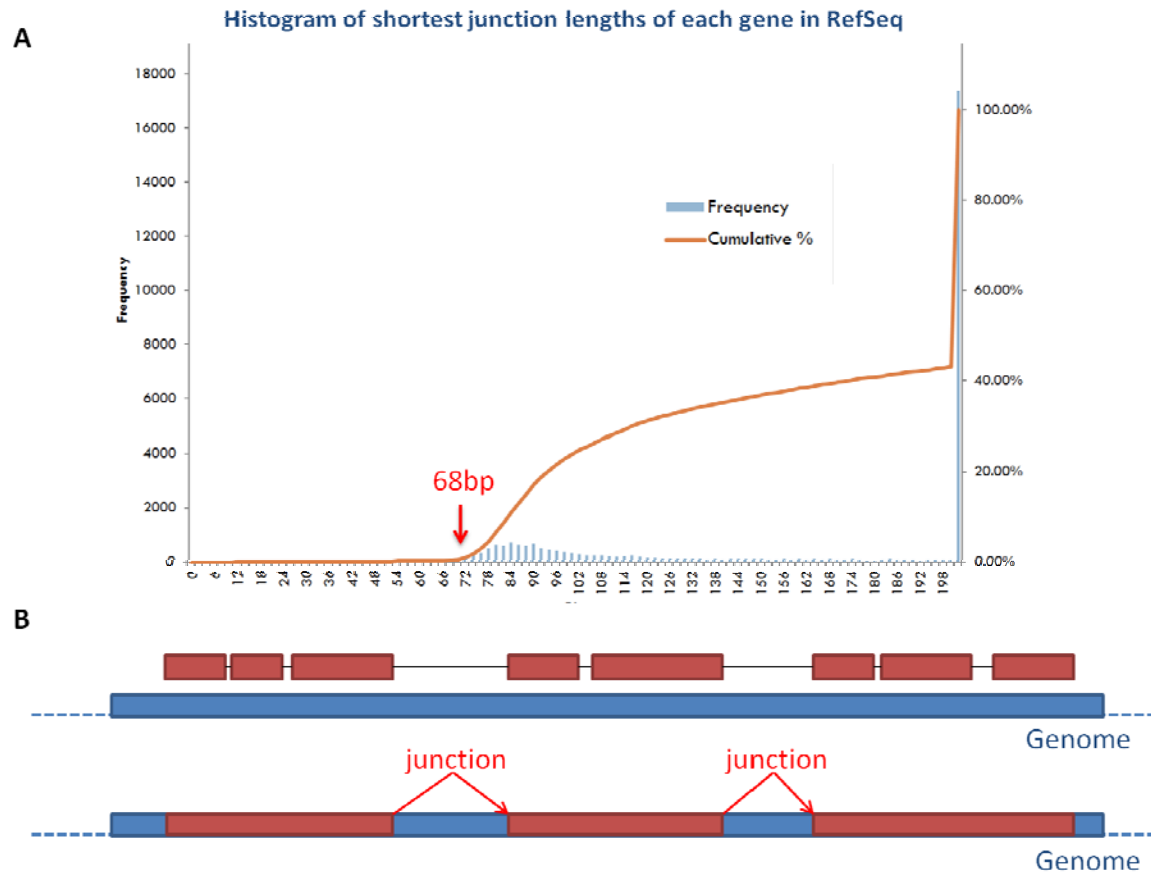


Figure S1. Flowchart of IDP.

IDP uses long reads and junctions as input. Direct detections and indirect predictions are identified.



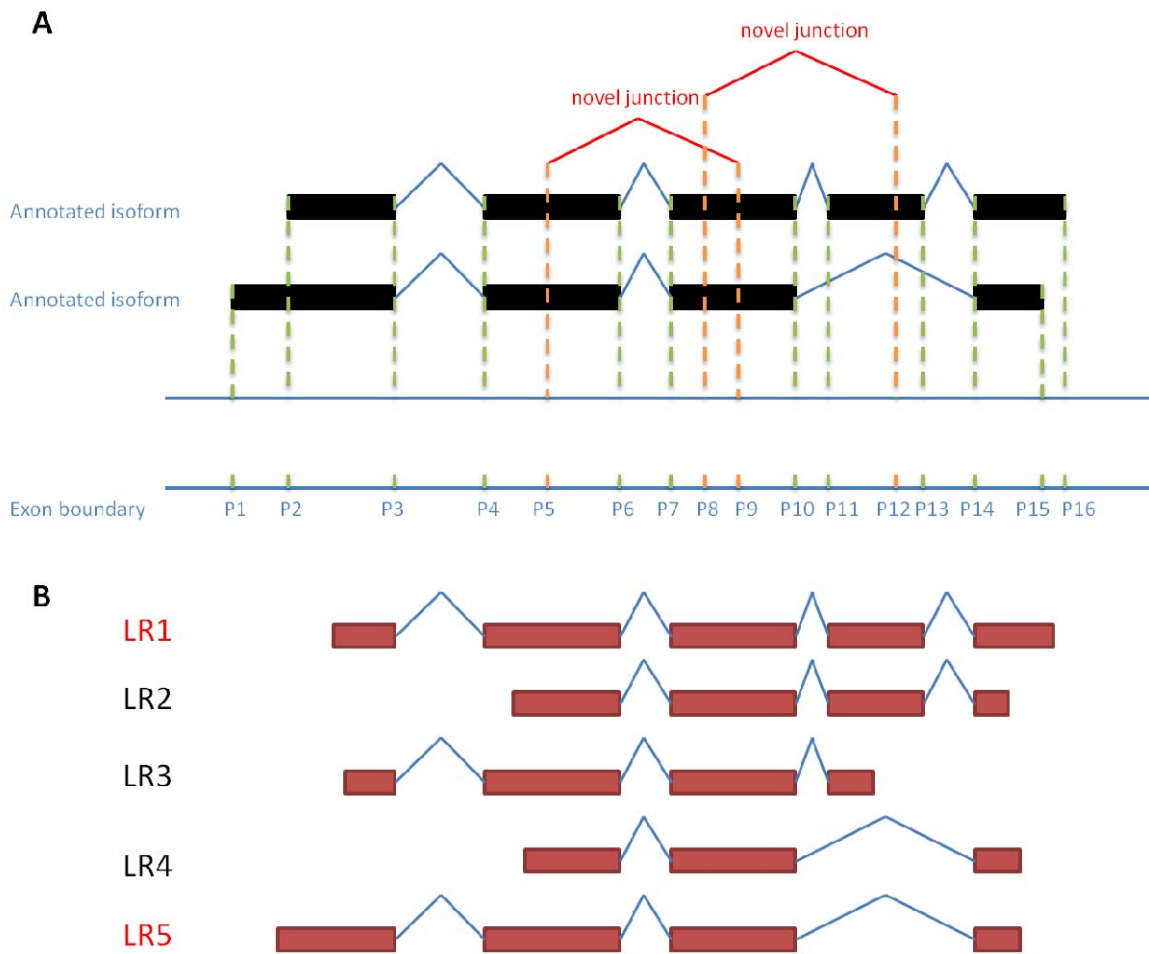


Figure S3. Definition of exon boundaries and nonredundant long reads

A) The splice sites and two ends (in blue and green) of annotated genes are used to define exon boundaries. Novel splice sites from SpliceMap are also included (in red and orange). Two flanking bases of exon boundary Pi are labeled as Pi- and Pi+. Isoform structure can be defined as an ordered set of exon boundaries. For example, two annotated isoforms have the exon boundaries ordered sets (from up to bottom) as

(P2+, P3-, P4+, P5-, P5+, P6-, P7+, P8-, P8+, P9-, P9+, P10-, P11+, P12-, P12+, P13-, P14+, P15-, P15+, P16-) and
(P1+, P2-, P2+, P3-, P4+, P5-, P5+, P6-, P7+, P8-, P8+, P9-, P9+, P10-, P14+, P15-)

B). Five long reads (from up to bottom) are denoted as

LR1: (P3-, P4+, P5-, P5+, P6-, P7+, P8-, P8+, P9-, P9+, P10-, P11+, P12-, P12+, P13-, P14+, P15-, P15+)

LR2: (P5-, P5+, P6-, P7+, P8-, P8+, P9-, P9+, P10-, P11+, P12-, P12+, P13-, P14+)

LR3: (P3-, P4+, P5-, P5+, P6-, P7+, P8-, P8+, P9-, P9+, P10-, P11+)

LR4: (P5-,P5+,P6-,P7+,P8-,P8+,P9-,P9+,P10-,P14+)

LR5: (P2-,P2+,P3-,P4+,P5-,P5+,P6-,P7+,P8-,P8+,P9-,P9+,P10-,P14+)

LR2 and LR3 are two proper subsets of LR1 and thus are redundant with LR1. LR4 is a proper subset of LR5. LR1 and LR5 are nonredundant, so they are selected.

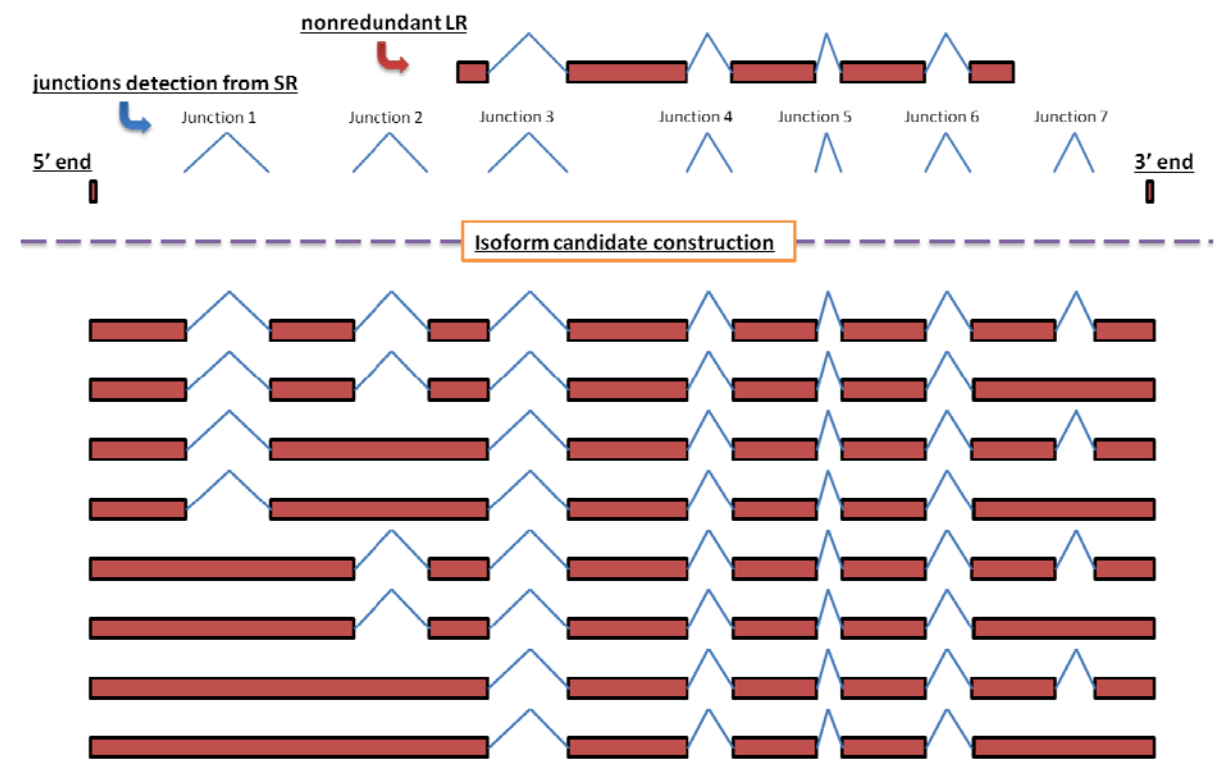


Figure S4. Isoform candidate construction from nonredundant long reads.

All possible junctions combinations are included until reaching the 5'end and 3'end. But the isoform candidates that contains exons longer than 1,700bp are excluded.

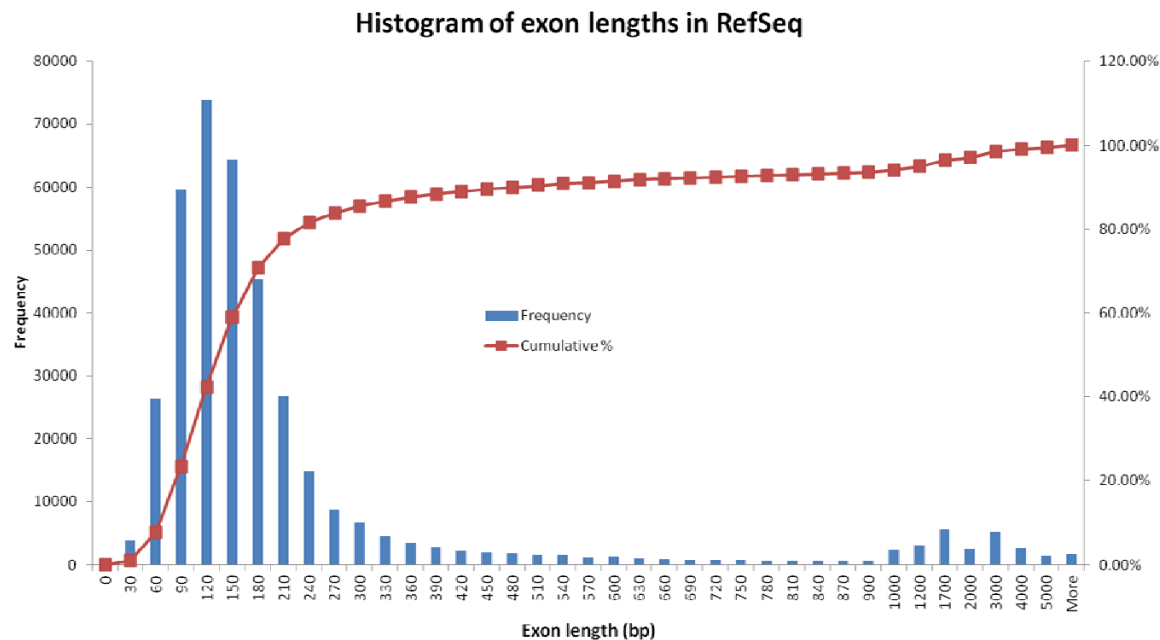


Figure S5. Distribution of exon lengths in RefSeq. >96% exons are longer than 17,000bp.

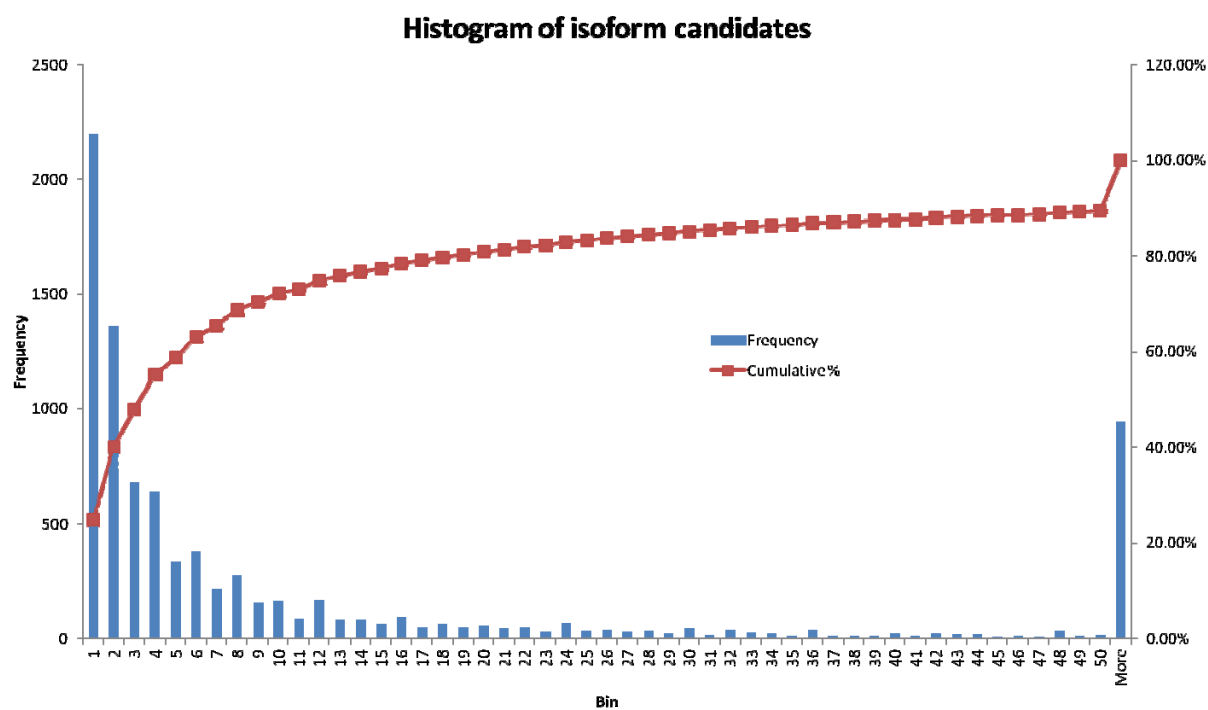


Figure S6. Distribution of number of isoform candidates constructed by IDP from hESC data.

About 90% gene loci have less or equal to 50 candidates and thus computable by MAP. Too many candidates may occur in some loci that are of low expression or of too long length, which may not likely to provide long reads cover enough junctions.

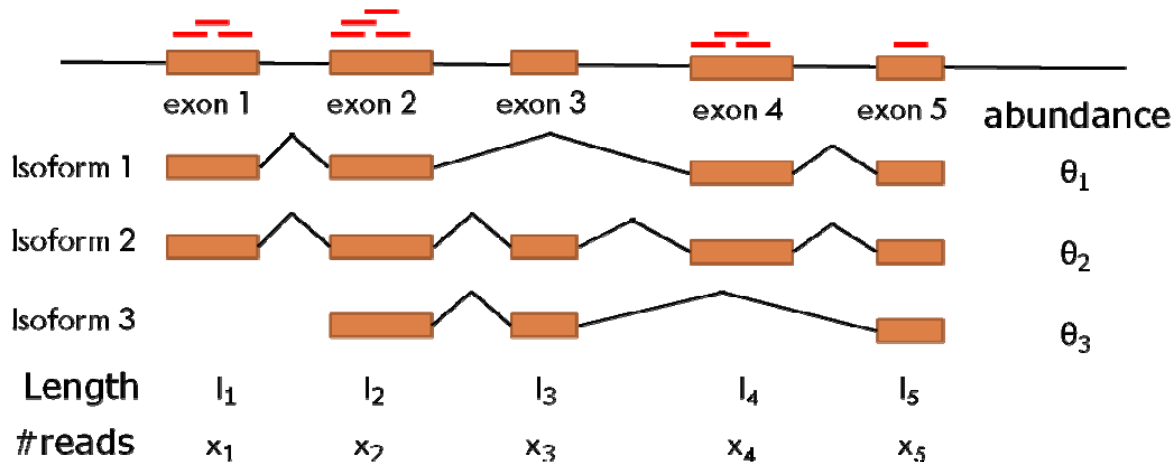


Figure S7. Possion model of short read coverage on gene isoforms.

X_s is the number of reads mapped to region s (exonic or junction region)

S is the set of all indexed regions.

H is the set of all isoforms.

$\Theta = \{\theta_h\}_1^H$ is the expression level of the set of isoform H .

$\lambda_s = N l_s \sum_h^H c_{sh} \theta_h$ and c_{sh} is the indicator of whether isoform h contains region s .

l_s is the length of region s .

N is the total number of mappable SRs.

Then, we assume $X_s \sim \text{Pois}(\lambda_s)$.

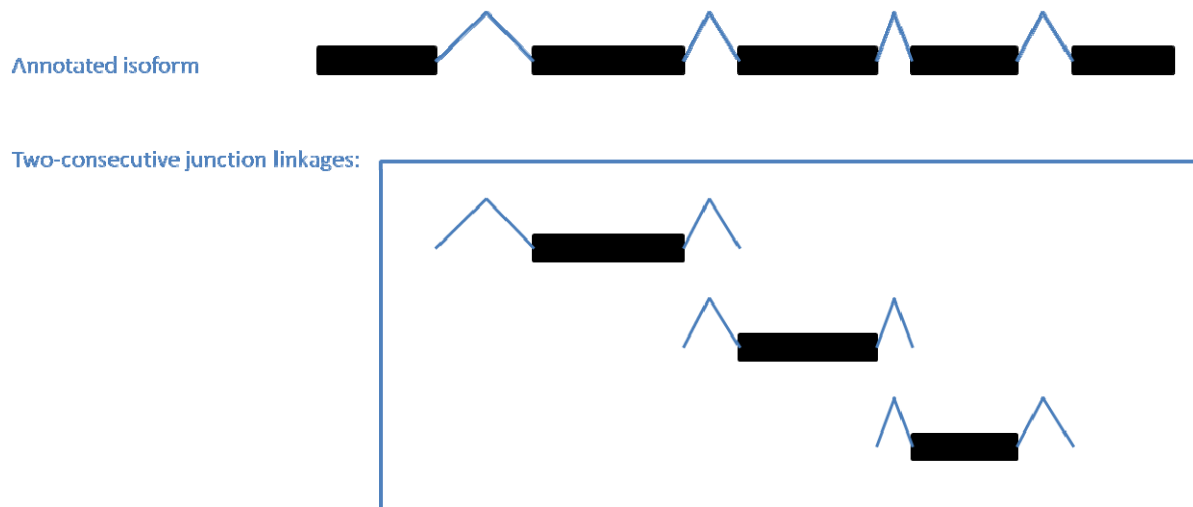


Figure S8. Three two-consecutive junctions linkages from an annotated isoform. Every two consecutive junctions within an isoform are counted as a linkage.

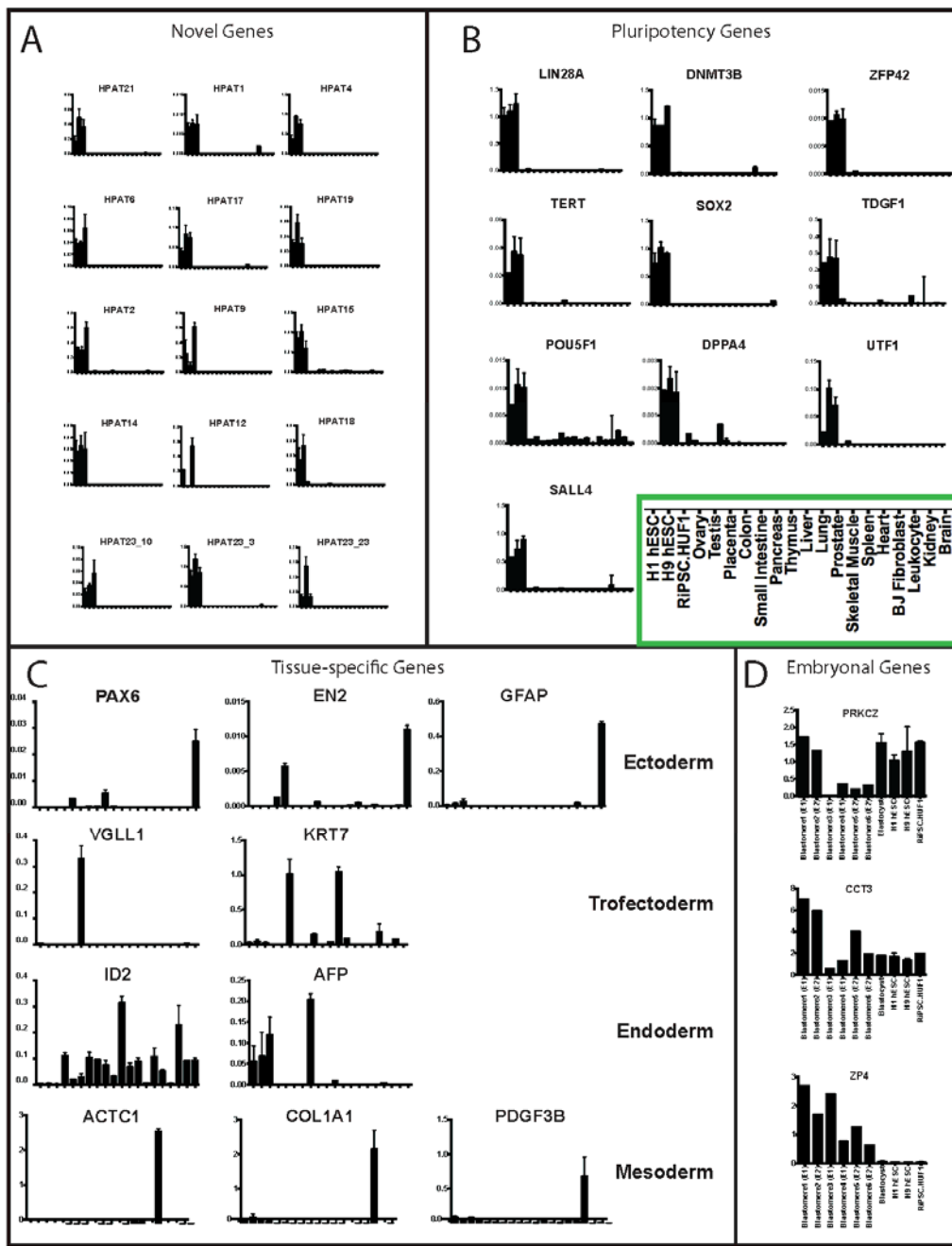
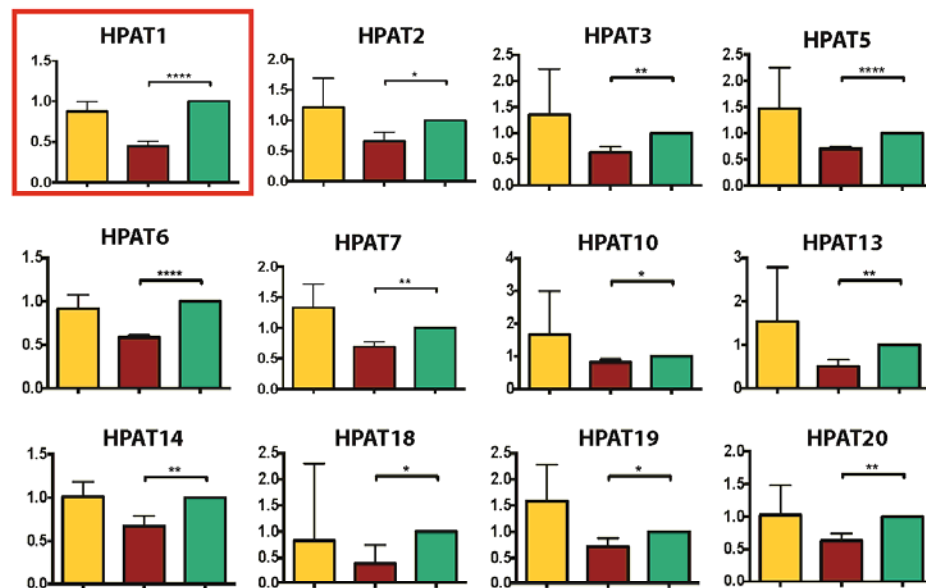


Figure S9. Gene expression validation of HPATs (refers to Figure 3)

- A. Gene expression analysis of HPAT by Q-PCR was performed on two hESC samples (H1 and H9), one iPSC line (RIPSC.HUF1) and a collection of cDNAs from fetal and adult tissues.
- B. Gene expression profiling of control pluripotency-associated factors.
- C. Gene expression profile of control tissue-specific markers.
- D. Gene expression profile of control embryonic-specific markers. The green box denotes the list of samples for panels A, B and C

A



B

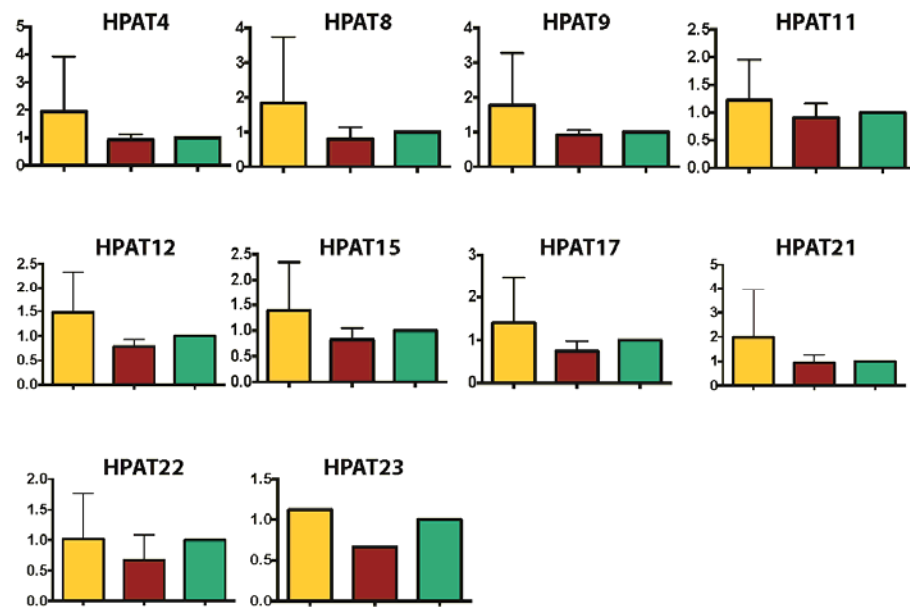


Figure S10. Functional effect of downregulation of HPAT genes (refers to Figure 4)

A. Gene expression analysis by Q-PCR of different HPATs after downregulation of GFP (negative control, in green), OCT4 (positive control, in yellow) and HPAT23_1 (in red).

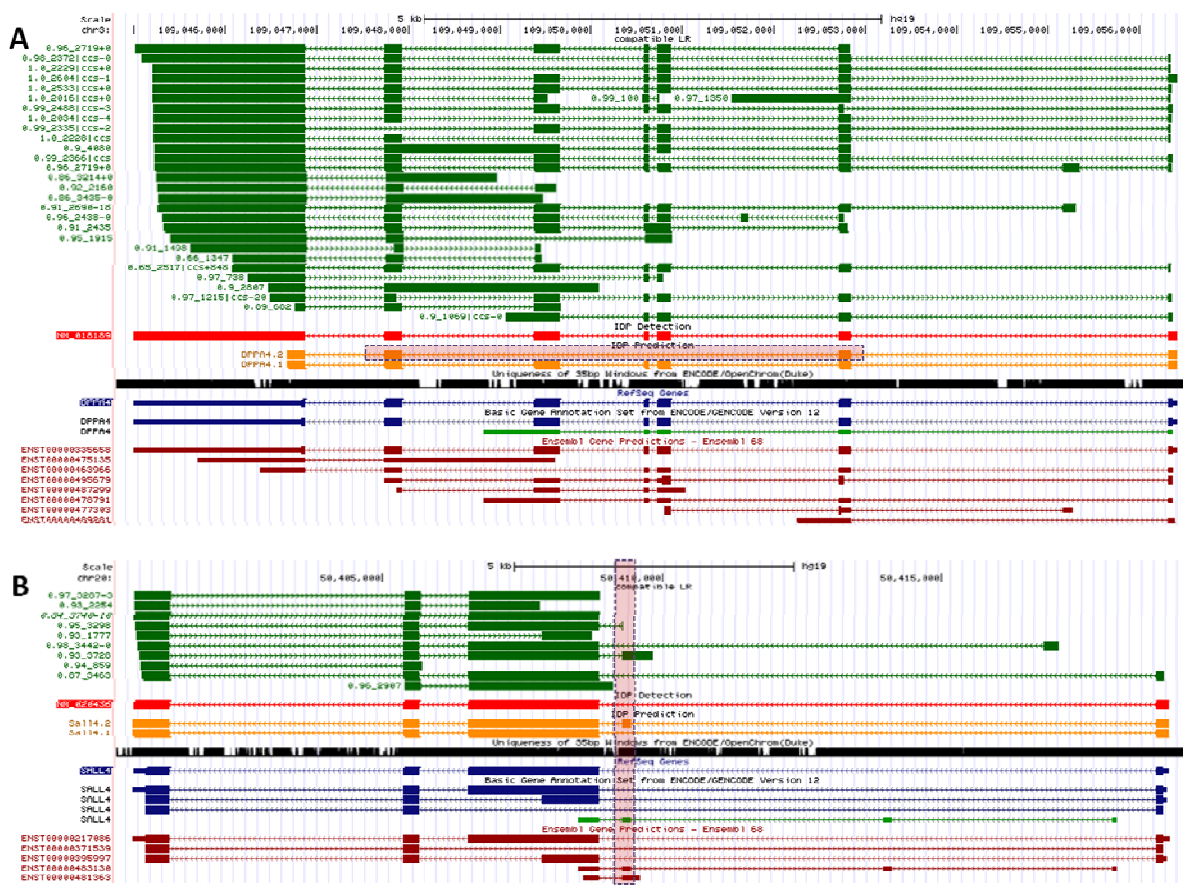


Figure S11. Novel isoform identifications in DPPA4 and SALL4. The browser setting is the same as in Figure 3 and Figure 4. The novel junction usages are highlighted in a pink dashed box.

A). The novel isoform of DPPA4 skips the exon 3, 4, 5 exon (from left to right) of the annotated isoform NM_018189.

B). Exon 4 (from left to right) of novel isoform SALL4.2 is not annotated in RefSeq but in Ensembl. The corresponding isoform ENST00000483130 is fragment of the IDP-identified isoform in hESC.

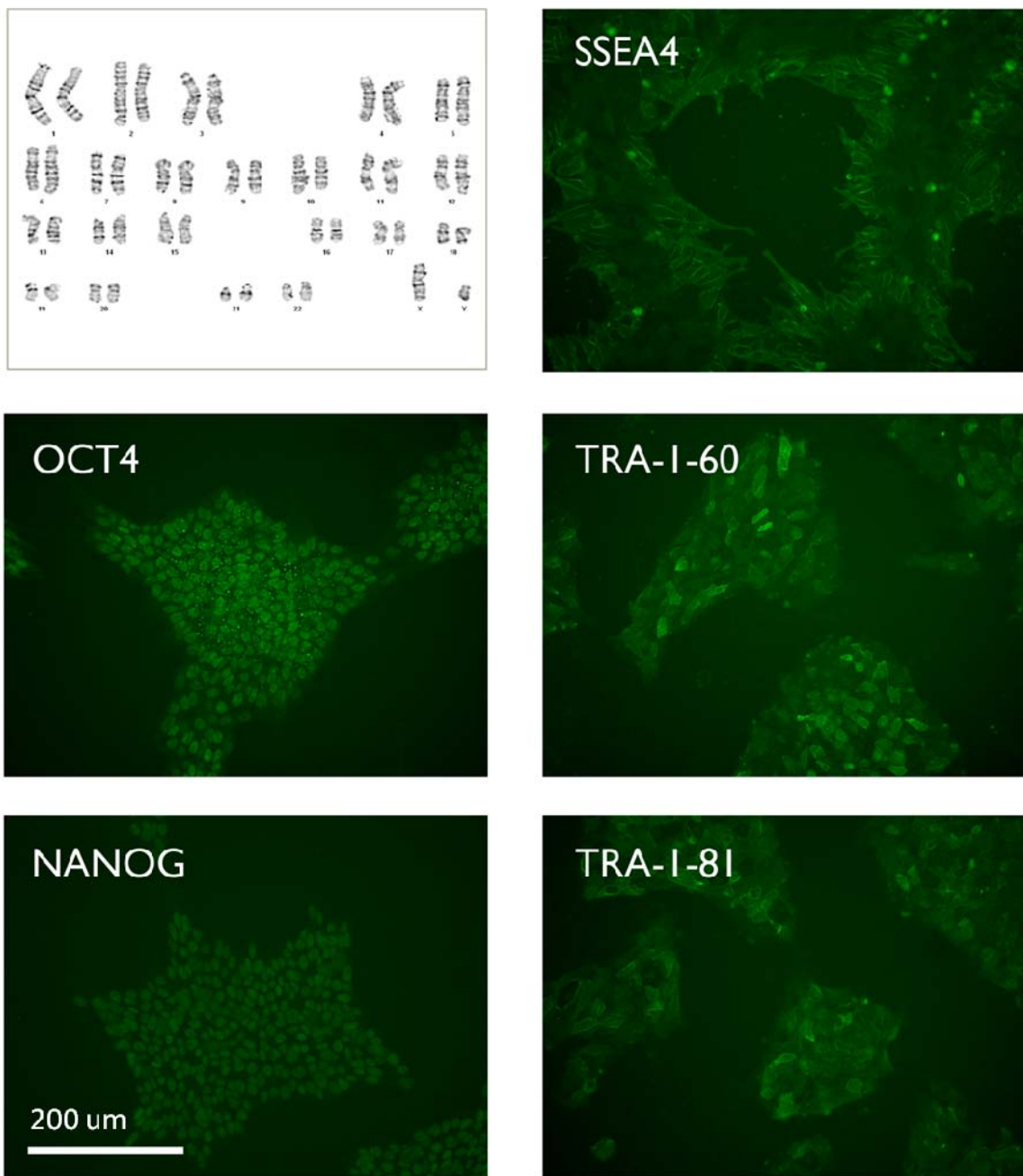


Figure S12. IF and karyotype.

This panel with the IF images proves the expression of some markers (OCT4, NANOG and the surface markers SSEA4, TRA-1-60 and TRA-1-81) of undifferentiated state of H1 and the normal karyotype.

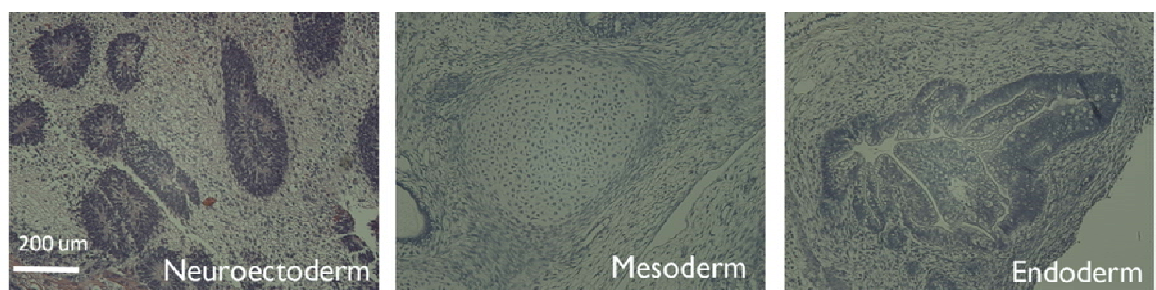


Figure S13. Teratoma assay of H1 cells.

Our H1 cells can form three germ layers: neuroectoderm, mesoderm and endoderm.

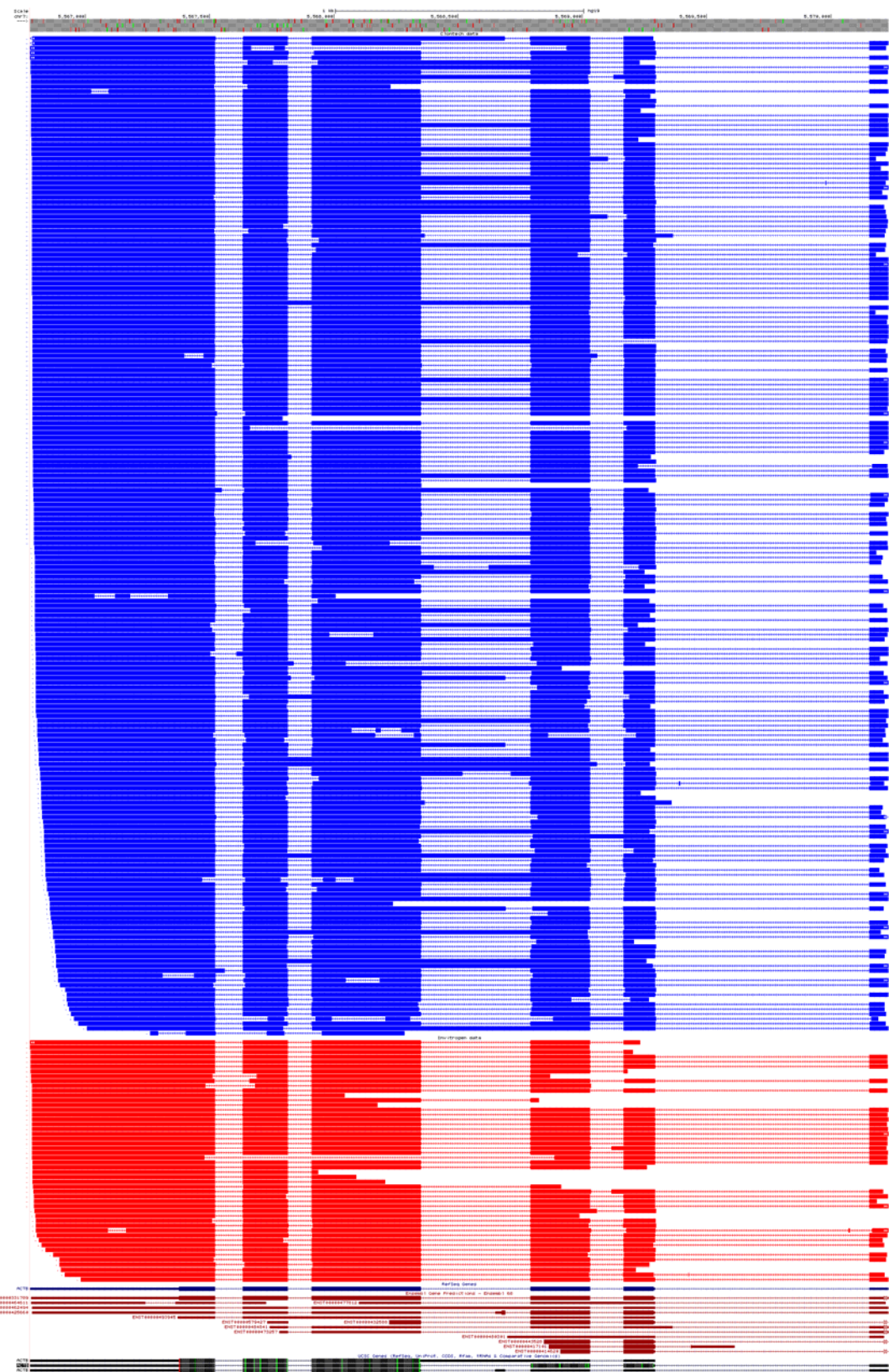


Figure S14. Full-length ACTB transcripts detected by Clontech and Invitrogen kits. Clontech is the blue track and Invitrogen is red.

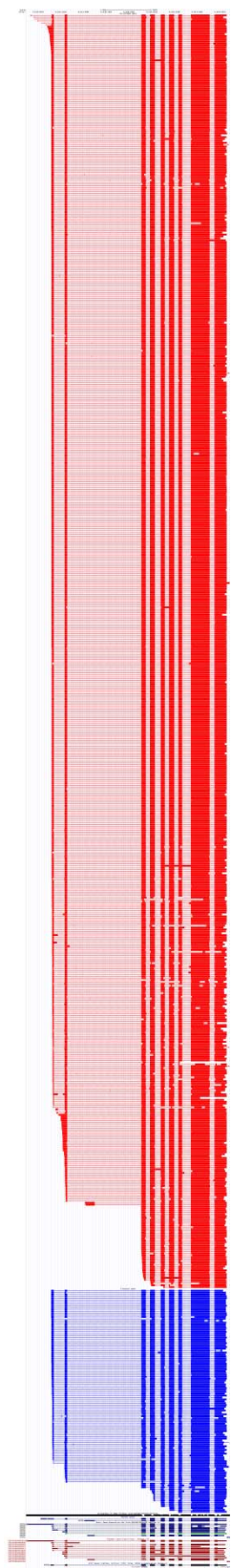


Figure S15. Full-length GAPDH transcripts detected by Clontech and Invitrogen kits. Clontech is the blue track and Invitrogen is red.

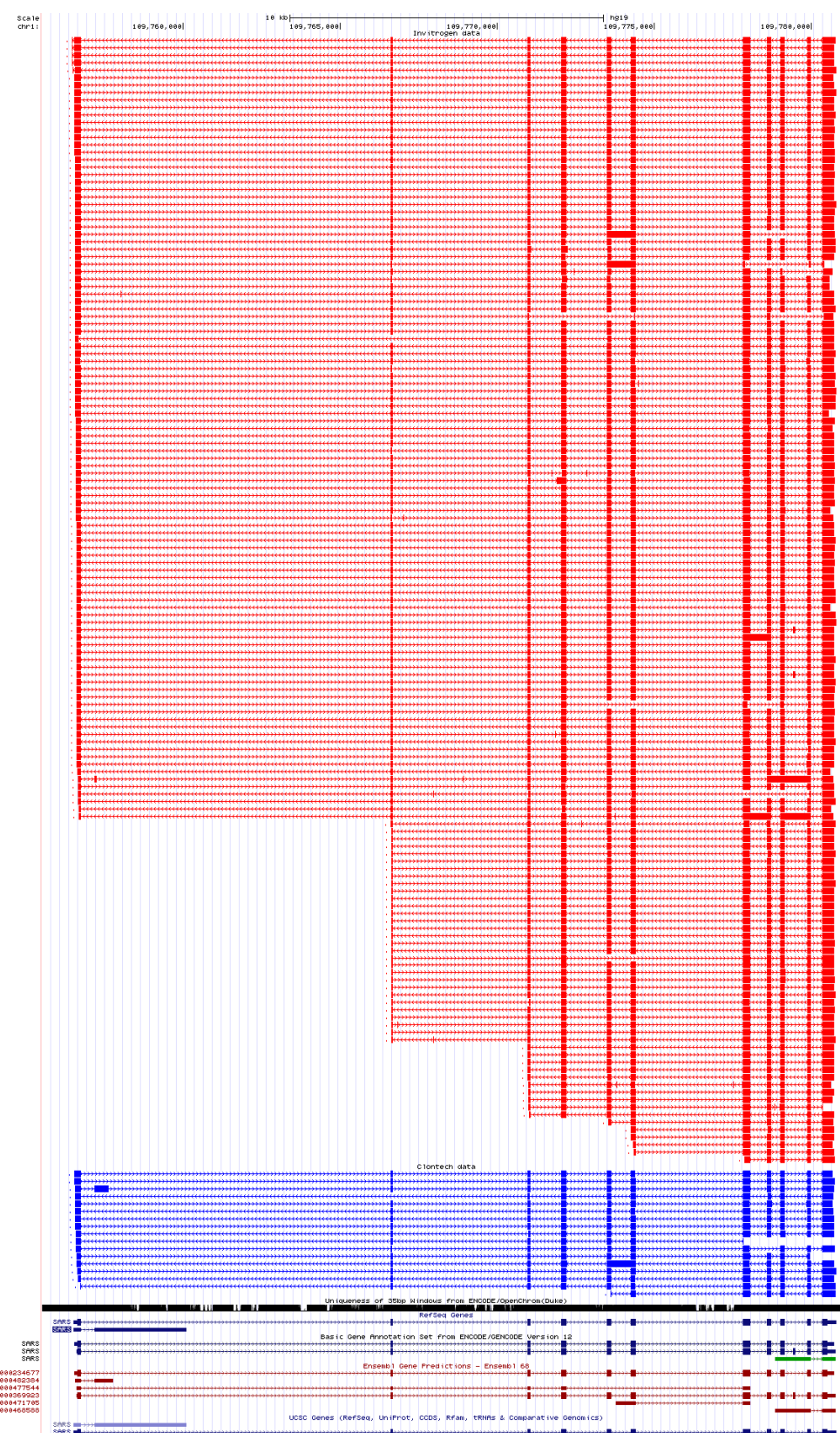


Figure S16. Full-length SARS transcripts detected by Clontech and Invitrogen kits. Clontech is the blue track and Invitrogen is red.

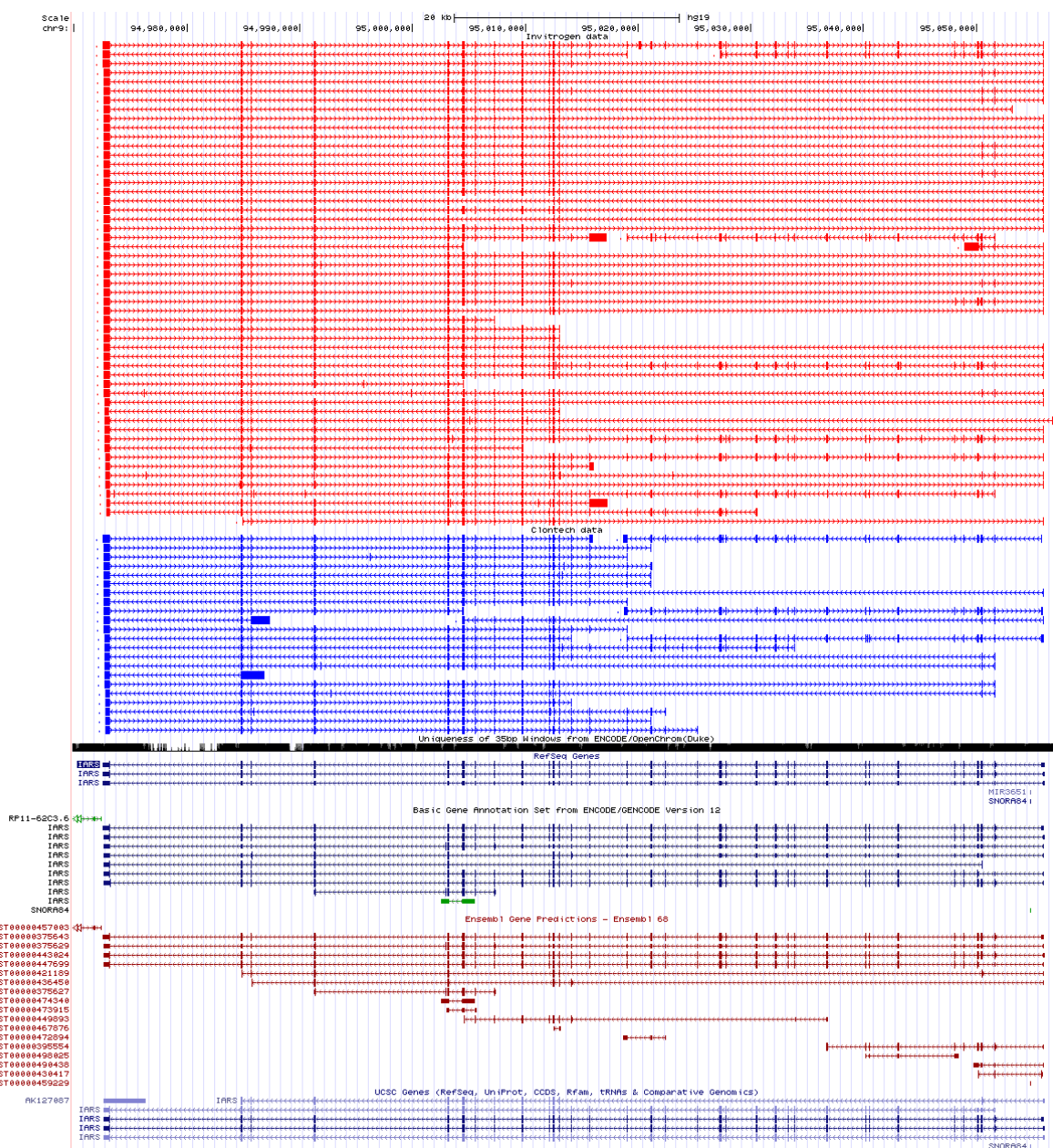


Figure S17. Full-length IARS transcripts detected by Clontech and Invitrogen kits. Clontech is the blue track and Invitrogen is red.